論文 / 著書情報
Article / Book Information

Title	The role of fines on internal instability and its impact on undrained mechanical response of gap-graded soils
Authors	Jitrakon Prasomsri, Akihiro Takahashi
Citation	Soils and Foundations, Vol. 60, Issue 6, pp. 1468-1488
Pub. date	2020, 12

HOSTED BY

ELSEVIER

Available online at www.sciencedirect.com

ScienceDirect

Soils and Foundations 60 (2020) 1468–1488

SOILS AND FOUNDATIONS

www.elsevier.com/locate/sandf

Technical Paper

The role of fines on internal instability and its impact on undrained mechanical response of gap-graded soils

Jitrakon Prasomsri, Akihiro Takahashi *

Department of Civil and Environmental Engineering, Tokyo Institute of Technology, Tokyo, Japan

Received 3 April 2020; received in revised form 11 September 2020; accepted 24 September 2020
Available online 24 October 2020

Abstract

This study presents an experimental investigation of the contribution of non-plastic fines to the development of seepage-induced internal instability and its impact on the undrained mechanical response of gap-graded sands. The purpose of the laboratory tests is to observe the internal instability of two key microstructures: (1) an underfilled microstructure in which the coarser particles control the stress transfer and (2) an overfilled microstructure in which the finer particles play a primary role in the stress transfer. Tests on medium dense sands with seven different fines contents are conducted using a pressure-controlled triaxial erosion device. The device enables internal erosion tests with high back pressure under a pressure-controlled condition. The results indicate that the initial fines content significantly affects the initiation and progress of internal instability. The phenomena of self-filtering and suffusion, evident for underfilled soil, can occur at relatively small hydraulic gradients. Depending on the initial fines content, overfilled soil is vulnerable to suffosion, seepage-induced failure, or an internally stable state, which can occur at large hydraulic gradients. Undrained compression tests on eroded soils reveal that suffusion makes the soil looser and more contractive, while suffosion makes the soil more dilative at large strain levels. As suffusion may create an unstable structure in the soils, sudden drops in deviator stress and sharp increases in pore water pressure and radial strain with axial straining are detected in all the post-suffusion soils at small strain levels. Finally, the identificaton of internal instability is illustrated in terms of the void ratio and the fines content, for assessing the initiation and progress of instability phenomena, as well as the possible soil microstructures.

Keywords: Sand; Fines; Internal erosion; Suffusion; Permeability; Triaxial compression test

1. Introduction

Seepage-induced internal instability is one of the mechanisms of internal erosion described by the loss of integrity in the soil by seepage flow and is associated with the transportation of soil particles. As a result, the instability can produce a modification of the soil microstructure, which can induce an alteration of the particle size distribution, porosity, and permeability, resulting in a change in the shear strength of the soil. This phenomenon has occurred in natural soil deposits and geotechnical structures, such as earth dams, dikes, and their foundations (*e.g.*, Stewart and Watts, 2000; Fell et al., 2003; Moffat and Fannin, 2011; Peng and Zhang, 2012; Yasuda et al., 2016; Razavi et al., 2020), one example being the sinkhole incident at the WAC Bennett Dam in 1996 (Stewart and Watts, 2000). The sinkhole was hypothesised to be a consequence of some form of internal erosion, where seepage water caused the downward migration of the finer material. A loss of fines can lead to the soil having a higher void ratio, after which an event or series of events may trigger its

Peer review under responsibility of The Japanese Geotechnical Society.
* Corresponding author at: Department of Civil and Environmental Engineering, Tokyo Institute of Technology, 2-12-1-M1-3 Oh-okayama, Meguro, Tokyo 152-8552, Japan.
E-mail address: takahashi.a.al@m.titech.ac.jp (A. Takahashi).

https://doi.org/10.1016/j.sandf.2020.09.008
0038-0806/

Nomenclature

D_r	relative density after preparation
D_{rc}	relative density after consolidation
e_c	global void ratio at end of consolidation or before erosion
e_e	global void ratio after erosion
e_s	inter-coarse void ratio before erosion
e_{se}	inter-coarse void ratio after erosion
e_{max}, e_{min}	maximum and minimum void ratios
$e_{s,\max}$	maximum void ratio of coarse particles
FC	initial fines content
FC_e	fines content after erosion
FC*	critical fines content
FC_{max}	maximum fines content
i,	hydraulic gradient
i_e	hydraulic gradient at initiation of erosion
k	permeability
k_i	initial permeability
k_e	end-of-test permeability
m_e	percentage of eroded soil mass
p'	mean effective stress
p'_i	initial mean effective stress
q	deviator stress
q_p,	deviator stress at peak
q_{ss}	deviator at quasi-steady state
u	pore water pressure
v	discharge velocity
W_f,	initial mass of fine fraction
W_c	initial mass of coarse fraction
ΔW_f	cumulative fines loss
$\Delta\varepsilon_a$	change in axial strain
$\Delta\varepsilon_r$	change in radial strain
$\Delta\varepsilon_v$	change in volumetric stain
σ'_a	effective axial stress
σ'_r	effective radial stress

collapse (Muir Wood, 2007). Seepage-induced internal instability is governed by the material properties, stress state, and hydraulic load conditions within the soil, none of which has been well understood. Moreover, the impact of internal instability on the mechanical soil responses has been disputed.

In past decades, internal instability was studied using gap-graded soils. These soils have been fundamentally correlated to a mixed microstructure for which the role of the fine particles varies with the fines content (Skempton and Brogan, 1994; Thevanayagam et al., 2002; Shire et al., 2014, 2016). Skempton and Brogan (1994) identified two important fines content (FC) parameters, namely, the critical fines content (FC*) and the maximum fines content (FC_{max}). The FC* is the fines content at which the fine particles fill the voids formed by coarse particles, estimated based on the maximum and minimum void ratios. The FC_{max} is the fines content at which the fine particles completely separate the coarse particles from one another. Skempton and Brogan (1994) proposed $FC_{max} = 35\%$. Thevanayagam et al. (2002) described four main microstructure cases based on the relationship between the void ratio and the fines content to categorise the liquefaction potential of bimodal silty sands. Based on a series of discrete element models (DEMs), Shire et al. (2014) suggested that each type of microstructure proposed by Thevanayagam et al. (2002) could be vulnerable to one of the three forms of internal erosion identified by Moffat et al. (2011). They stated that, for Cases *i* – *iii* using the classification method by Thevanayagam et al. (2002) for soils with $FC < FC$*, which are often referred to as "underfilled" (fines are confined within the voids between the coarse particles) by ICOLD (2013), if the material criterion is met, these soils are susceptible to suffusion. For Case *iv*, on the other hand, using the same classification method for soils with $FC > FC$*, which are referred to as "overfilled" (a matrix of fines disperses the coarse particles), these soils are in an *internally stable* state, but could be vulnerable to other forms of internal erosion, such as piping.

The progress of internal instability has been characterised by several phenomena, considering the changes in permeability and volumetric deformation. Moffat et al. (2011), for example, suggested that instability could be characterised by three phenomena: suffusion, suffusion, and piping. Subsequently, Fannin and Slangen (2014) and Slangen and Fannin (2017) suggested that *suffusion* describes seepage-induced mass loss accompanied by increasing permeability and no marked change in volume, while *suffosion* describes seepage-induced mass loss accompanied by a contractive change in volume. Some researchers have revealed that, along with the progress of suffusion, the detachable particles cause an increase in the size and number of pore throats, leading to an increase in permeability (Chang and Zhang, 2011; Ke and Takahashi, 2012; Sibille et al., 2015). In contrast, if the size of the pore throat openings is not large enough to allow the detachable particles to pass through them, the finer particles may become clogged. This is why some researchers have observed diminishing permeability, which is sometimes called *self-filtering* (Bendahmane et al., 2008; Marot et al., 2009; Reddi et al., 2000; Xiao and Shwiyhat, 2012). The hydraulic loading history has been found to play an essential role in the progress of suffusion (Rochim et al., 2017). Bonelli (2012) concluded that suffusion and self-filtering are two coupled processes of internal instability that are governed by the geometry of the porous

network (*e.g.*, soil microstructure), the interaction between the solid and fluid phases, and the hydraulic conditions, all of which remain unclear.

Although internal instability phenomena have been widely investigated in the past decade, experimental examinations of the impact of internal instability on the mechanical soil responses have been quite limited. Several researchers performed drained monotonic compression tests on eroded soils (Chang and Zhang, 2012; Ke and Takahashi, 2014b, 2015). They found that originally dilative soil would turn into contractive soil after a significant loss of fines, leading to smaller drained strength. Other researchers performed post-erosion undrained triaxial compression tests on gap-graded soils (Xiao and Shwiyhat, 2012; Ke and Takahashi, 2014a; Ouyang and Takahashi, 2015; Mehdizadeh et al., 2017). Contrary to the expectations, larger undrained shear strength and stiffness were observed in their tests. They reported that the soils became less contractive after erosion. This larger shear strength of eroded soils may be mainly attributed to the coarser particle rearrangement accompanied by a reduction in volume.

In this paper, the authors report an experimental investigation of the influence of fines on the seepage-induced instability of gap-graded sands with seven different fines contents. The microstructure type of each soil is established. The experiments are conducted using a pressure-controlled triaxial erosion apparatus. The seepage-induced instability phenomena are then characterised for each soil based on the measurement of the fine particle loss, volume change, and permeability. Finally, the impact of the instabilities on the undrained mechanical response of these sands is also investigated.

2. Laboratory experiments

2.1. Testing materials

Gap-graded mixtures of Silica sand No. 3 and coloured Silica sand No. 8 are used as the test materials. The particle shape characteristics of these sands are quantified using a digital microscope, VHX-6000, with image processing software. The shape measurements are the aspect ratio (Ar), sphericity (Sp), and convexity (Cx); their definitions are given in Altuhafi et al. (2013). Altuhafi et al. (2013) proposed a particle classification based on the relationship between Cx and Sp, which has been validated with the classification provided by Power (1953). The particle shape of Silica sand No. 3, as the coarse fraction, is nominally identical to a median aspect ratio (Ar_{50}) of 0.73, median convexity (Cx_{50}) of 0.95, and median sphericity (Sp_{50}) of 0.86. The particle shape of Silica sand No. 8, as the erodible fines fraction, is slightly more angular, with Ar_{50} of 0.65, Cx_{50} of 0.92, and Sp_{50} of 0.83. Based on the indices of particle shape, Silica sand Nos. 3 and 8 are categorised as sub-angular and angular, respectively, according to Altuhafi et al. (2013). It should be noted that Silica sand No. 8 is non-plastic and regarded as fines in this study, although the particle size of this sand is larger than that of fines according to the definition given by the Unified Soil Classification System (ASTM D2487-11, 2012); fine-grained soil is defined as soil that passes through Sieve No. 200 (75 μm). Silica sand No. 3 alone and seven mixtures with fines contents of 15, 20, 25, 30, 32.5, 35, and 40% (by mass) are used in this study. The particle size distributions of the silica sands and the mixed samples are presented in Fig. 1. The gradation properties of the silica sands and the mixtures are summarised in Table 1. The susceptibility of the internal instability of the mixtures is assessed by the selected available methods, which are based on filter rules and a shape analysis of the grading. The results of the assessment are summarised in Table 2, showing that the mixtures are mostly unstable.

2.2. Triaxial erosion apparatus

The triaxial erosion apparatus, located at the Soil Mechanics Laboratory of the Department of Civil and Environmental Engineering, Tokyo Institute of Technology, was developed initially by Ke and Takahashi (2014a), and then revised and used to conduct the tests. A schematic diagram of the apparatus is provided in Fig. 2. The device mainly consists of an automated triaxial system, a revised seepage control system, and an eroded soil collection unit. The revised seepage system in the current apparatus is based on the principle of hydraulic head control, in which the internal erosion experiments can be performed with high back pressure under a pressure-controlled condition. The hydraulic head control system has been widely used in erosion testing (*e.g.*, Bendahmane et al., 2008; Chang and Zhang, 2011; Slangen and Fannin, 2017), and is conceptually different from the flow control system adopted by Ke and Takahashi (2014a).

The seepage control system is designed to apply the differential hydraulic head between the top and the base of the sample. The inlet tank is used to impose the seepage

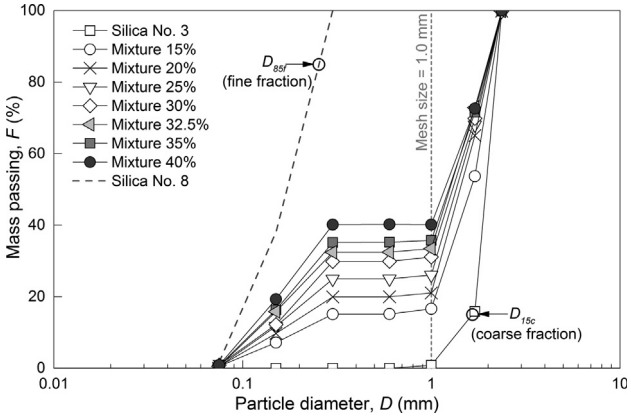

Fig. 1. Particle size distribution curves of soils.

Table 1
Physical and gradation properties of test materials.

Physical and gradation properties	Silica sand		Mixture (%)						
	No. 3	No. 8	15	20	25	30	32.5	35	40
Specific gravity, G_s	2.645	2.645	2.645	2.645	2.645	2.645	2.645	2.645	2.645
Maximum void ratio, e_{max}	0.98	1.24	0.79	0.76	0.73	0.70	0.70	0.72	0.73
Minimum void ratio, e_{min}	0.75	0.88	0.54	0.48	0.44	0.40	0.41	0.42	0.43
Uniformity coefficient, C_u	1.47	2.18	9.27	10.49	11.41	11.35	12.4	12.65	13.09
Curvature coefficient, C_c	1.60	0.98	4.30	5.09	5.35	1.98	0.45	0.38	0.31
D_{15c} (mm)[a]	1.65	–	–	–	–	–	–	–	–
D_{85f} (mm)[b]	–	0.25	–	–	–	–	–	–	–
$(H/F)_{min}$[c]	–	–	0.94	0.81	0.62	0.49	0.45	0.37	0.28
Soil classification, *USCS*[d]	SP	SP	SM	SM	SM	SM	SM	SM	SM
Particle description	Sub-angular ~ Angular								

Note:
[a] D_{15c} is the particle diameter through which 15% by mass of the coarse particles passed.
[b] D_{85f} is the particle diameter through which 85% by mass of the fine particles passed.
[c] F is the passed fraction by mass finer than d, and H is the mass fraction between d and $4d$ (Kenney and Lau, 1985, 1986).
[d] The mixtures are classified as silty sand (SM) regarding Silica No. 8 as fines.

flow throughout the sample in a downward direction. The pore water pressure (PT#3) at the inlet tank is herein called "inlet tank pressure (*ITP*)"; it is automatically operated with the accuracy of ±0.2 kPa. Constant pore water pressure (PT#1) is maintained at the base of the sample and is herein called "base pressure (*BP*)"; it is operated with the accuracy of ±0.1 kPa. The pressure transducer (PT#2) on the top of the sample (*TP*) is installed to measure the actual head drop in the sample, excluding the head loss in the fittings and tubes, and is herein called "top pressure (*TP*)"; it has the accuracy of ±0.1 kPa. The flow rate through the sample is measured on the top by a flow meter (FR) with the accuracy of ±0.08 cm^3/min, and further used to derive the discharge velocity (v) considering the current sample's cross-section. The recorded parameters comprise the pore water pressure, flow rate, axial strain, radial strain, deviator stress, and cumulative eroded soil mass. The hydraulic gradient (i) is calculated using the differential pressure between *TP* and *BP*. The volume change (ε_v) is estimated using the axial and radial displacements; the accuracy of the axial and radial strains are ±0.03% and ±0.02%, respectively, or about ±0.06% volumetric strain derived from the uncertainty of the measured quantities and the propagation of uncertainty (ASTM E2655-08, 2008). The permeability (k) is obtained from Darcy's equation. The eroded soil mass (m_e) is the ratio of the mass of eroded fines measured by the miniature load cell (LC#2), with the accuracy of ±0.1 g, to the initial mass of the fine fraction.

It should be noted that the current testing apparatus applies a downward seepage flow, in which the flow direction is the same as the direction of gravity. Consequently, the erosion of fines may be greater and initiated more easily than when the testing apparatus applies an upward seepage flow, since an upward seepage force needs to overcome the gravitational force. In a practical situation, the testing model could replicate the lower reservoir level of an earthen dam that may induce the downward erosion of the dam material, which could lead to the occurrence of sinkholes.

2.3. Test procedures

The samples are prepared by the under-compaction moist tamping method introduced by Ladd (1978), with an initial moisture content of 10%, to avoid the segregation of the two different particle sizes. Uniformity of the sample is controlled by the nonlinear average under-compaction criterion proposed by Jiang et al. (2003). After tamping, the dimensions of the cylindrical samples are a height of 150 mm and a diameter of 75 mm. Micro-observations are then performed to further inspect the segregation of the particles, as shown in Figs. 3 and 4, capturing the top surface of the samples after their preparation. It is seen

Table 2
Summary of assessment results of internal instability.

Based on	References	Internally unstable if	Mixtures (%)						
			15	20	25	30	32.5	35	40
Filters rule	Kézdi (1979)	$(D_{15c}/D_{85f})_{max} \geq 4$	U	U	U	U	U	U	U
Shape analysis	Kenney and Lau (1986)	$(H/F)_{min} \leq 1.0$	U	U	U	U	U	U	S
	Li and Fannin (2008)	$(H/F)_{min} \leq 1.0$ and $H < 0.15$	U	U	U	U	U	U	U

Note: U is unstable and S is stable.

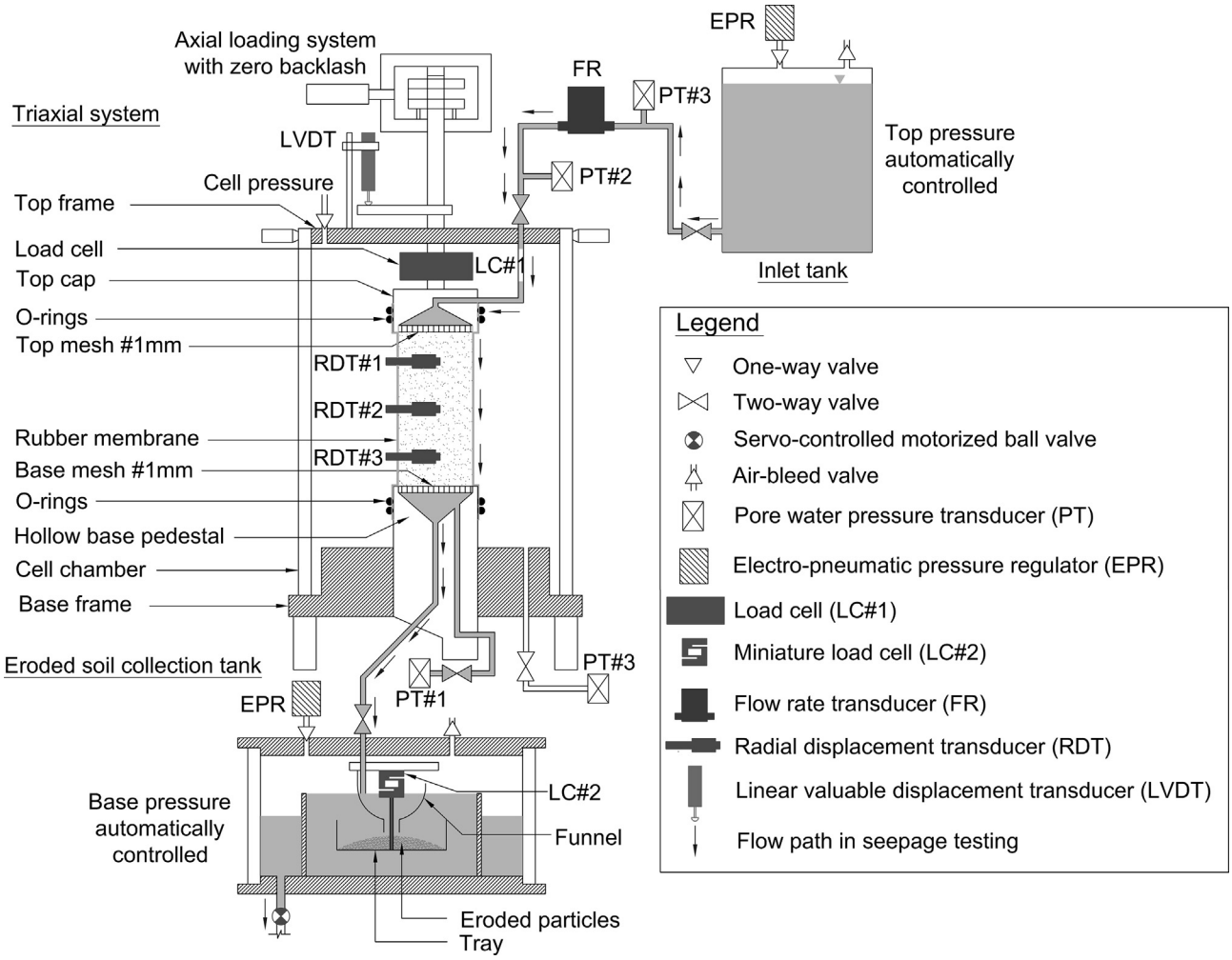

Fig. 2. General configuration of modified triaxial erosion apparatus.

that, with the help of a small amount of water, the coarse particles are coated by fines even in the case of a fines content of 15%. This suggests that the role of fines is not simply to occupy the void spaces formed by the coarse skeleton when the samples are prepared by the moist tamping method. Moreover, the moisture content of 10% is in the range of the ideal moisture content (7–13%), introduced by Pachideh and Hosseini (2019), which was found to effectively lessen the segregation.

Back pressure (*BP*) of 400 kPa is applied to ensure complete saturation; a *B*-value of greater than 0.95 is achieved. The samples are then consolidated to the mean effective stress (p'_i) of 50 kPa. The purpose of conducing the tests under low effective stress is to understand the internal erosion mechanism and the potential for the deformation or failure of the soil because of internal erosion at shallow depths, i.e., sinkholes. The seepage is imposed by increasing the *ITP* from 400 to 430 kPa at a rate of 2 kPa/min, keeping it constant for 30 min, and then decreasing it to 400 kPa at the same rate. The *BP* of 400 kPa is maintained throughout the tests. Zero-deviator stress is kept constant during the erosion tests. After erosion, a *B*-value of greater than 0.95 is still maintained.

Then, an undrained compression test with the axial strain rate of 0.1%/min is performed. Corrections regarding changes in the cross-sectional area and membrane penetration during the shearing are carried out. The testing programs and their major parameters are summarised in Table 3. The test ID in the following is either WE_FX or WOE_FX, for which WE and WOE represent samples with and without erosion, respectively. X is the percentage of initial fines content (*FC*) by mass. It should be noted that the fines content by mass is the same as that by volume since the specific gravity of all the particles is the same. In the following, *FC* is also used as the fines content by volume.

3. Microstructure identification

It has been widely recognised that, as the proportions of the coarse and fine particle contents of the soil change, the nature of the microstructure also changes (Yamamuro and Covert, 2001; Thevanayagam and Mohan, 2000; Thevanayagam et al., 2002). A change in microstructure leads to a different particle contact network and force chain along with the contacts between particles. Therefore, a

different microstructure would exhibit different seepage responses and mechanical behaviour.

In this study, digital microscopic images are also used to observe the interaction between the fine and coarse particles as supplemental evidence when discussing the microstructure of the mixtures. As menntioned above, Figs. 3 and 4 show the micro-observations of the samples for different FC and initial void ratio (e_i) values. It can be seen that, for the host sand sample, WE_F0, the coarse particles are in contact with each other (see Fig. 3a). By adding a small amount of fines (i.e., WE_F15), the fines cling to the surface of the coarse particles and the coarse particles are mainly in contact with each other (see Fig. 3b). For WE_F20 and WE_F25, the fine particles are in contact with each other and occupy locations between the coarse particles (see Fig. 3c and d). For the transitional sample, WE_F30, the fine particles seem to occupy and be tightly packed into the voids between the coarse particles (see Fig. 4a). For WE_F32.5, WE_F35, and WE_F40, the coarse particles are floating in the fines matrix, such that most of them are separated far apart from each other and lose contact (see Fig. 4b–d).

Thevanayagam and Mohan (2000) proposed an intergranular matrix phase diagram, expressed in terms of the fines content, global, inter-coarse, and inter-fines void ratios, to explain the interaction of the coarse and fine particles in a soil microstructure of gap-graded soil. Fig. 5 shows the intergranular matrix phase diagram of the mixtures created in this study; zones separate the void ratio – fines content (e – FC) space into four cases (*i*, *ii*, *iii*, and *iv*). In the figure, the minimum and maximum void ratios (e_{min} and e_{max}), determined by the procedures proposed by Lade et al. (1998), are plotted and considered as the densest and loosest states of the mixtures, respectively. The solid lines on the left-hand side denote the inter-coarse void ratios of the mixture (e_s) and can be expressed by

$$e_s = \frac{e + FC}{1 - FC} \tag{1}$$

where e = global void ratio and FC = fines content. The dashed lines on the right-hand side denote the inter-fines void ratios of the mixture (e_f) and can be expressed by

$$e_f = \frac{e}{FC} \tag{2}$$

The void ratio defined by Eq. (1) can characterise the soil behaviour of the "underfilled" soils with smaller fines contents, while the void ratio defined by Eq. (2) can characterise the soil behaviour of the "overfilled" soils with larger fines contents. There is also a certain transitional zone between these two; the transitional fines content can be estimated at around 28.4–30.5% by the intersections between e_s and e_f. In the experiment, e_{max} and e_{min} reach a minimum value around FC = 30%, which is considered as FC* in this study. In cases (*i*) through (*iii*), as $FC < FC$*, the soils have an "underfilled" microstructure; the coarse particle contacts play a primary role in the soil matrix, while the finer fraction offers a minor contribution. In the transitional zone, as $FC \approx FC$*, the microstructure is "filled"; both coarse and fine particles may fit and be tightly packed in the soil matrix (Shire et al., 2016). For case (*iv*), as the condition of $FC > FC$* yields an "overfilled" microstructure, the matrix of the fine particles plays the primary role in the seepage and strength characteristics of the soil.

For each test, the initial microstructure is defined by plotting the soil state after consolidation on the diagram shown in Fig. 5. The soil state is defined by the initial FC and the global void ratio at the end of consolidation (e_c). Based on the micro-observations in Figs. 3 and 4, and the soil state in the intergranular matrix phase diagram in Fig. 5, it is postulated that the microstructures of WE_F15, WE_F20, and WE_F25 are "underfilled" [Cases *i* and *iii* by Thevanayagam and Mohan (2000)]. WE_F30 is a "filled" microstructure [Case *iii* or *iv*]. WE_32.5, WE_F35, and WE_F40 have "overfilled" microstructures [Case *iv*]. As mentioned above, Table 3 summarises the major parameters before erosion testing and the possible microstructures. It should be noted that the target relative density after the sample preparation (D_r), determined by Eq. (3), is 50%, but that the relative density before erosion (D_{rc}), determined by Eq. (4), is larger than D_r since e_c is smaller than e_i.

$$D_r = \frac{e_{\max} - e_i}{e_{\max} - e_{\min}} \tag{3}$$

$$D_{rc} = \frac{e_{\max} - e_c}{e_{\max} - e_{\min}} \tag{4}$$

4. Erosion test results and analysis

4.1. Typical test results

In total, eight erosion tests are performed on medium dense sand samples at p'_i = 50 kPa. The test results are summarised in Table 3. The variation in fines for each test, caused by internal erosion, is summarised in Table 4. The performance of WE_F25 is presented in the following as an example. The evolutions of ITP, TP, BP, i, m_e, ε_v, v, and k are illustrated in Fig. 6.

WE_F25 is the sample categorised as underfilled soil (Case *iii*) with the initial FC = 25% and e_c = 0.59. When ITP is increased, the variation in i exhibits a nonlinear response. It is followed by a gradual decrease in i when ITP remains constant, as shown in Fig. 6a. This response is due to the combined effect of self-filtering and the wash out of suspended particles from the sample. In this case, the hydraulic gradient required to initiate internal erosion (i_e), determined by the first detection of m_e, is 0.86. The values for i_e of all the eroded samples with different FC are summarised in Table 3, indicating that the onset of internal erosion depends on the initial FC.

The evolution of m_e in Fig. 6b indicates that the fines are eroded from this sample. Typically, m_e increases rapidly in

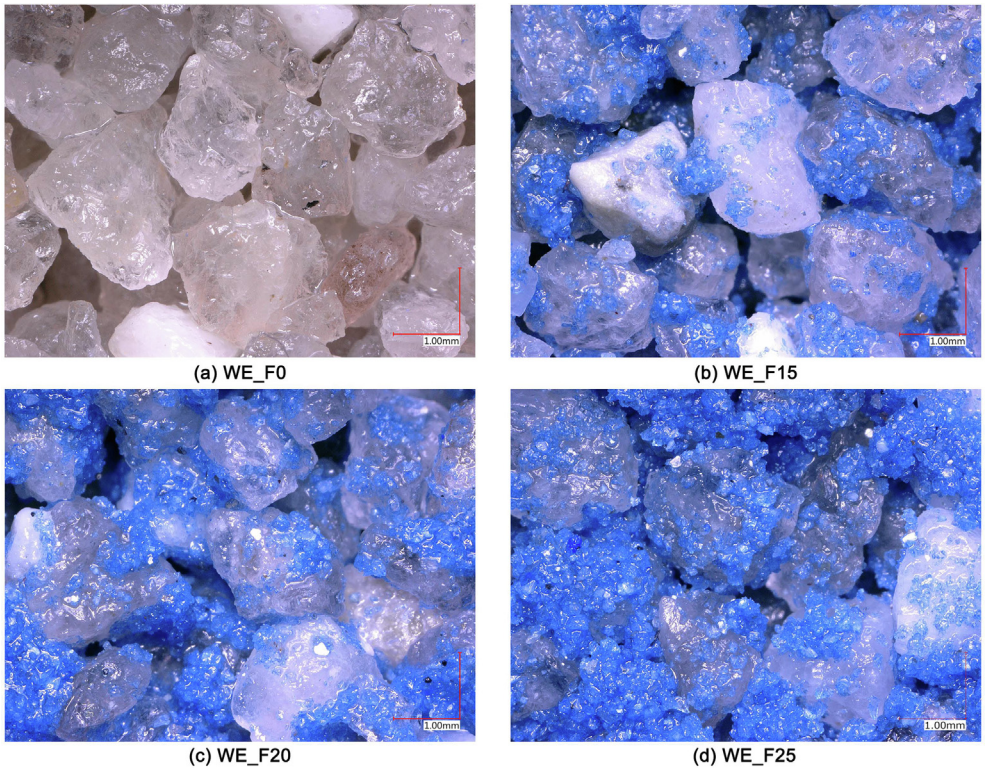

Fig. 3. Microstructure of soils after sample preparation for $FC < 30\%$: (a) WE_F0, (b) WE_F15, (c) WE_F20, and (d) WE_F25.

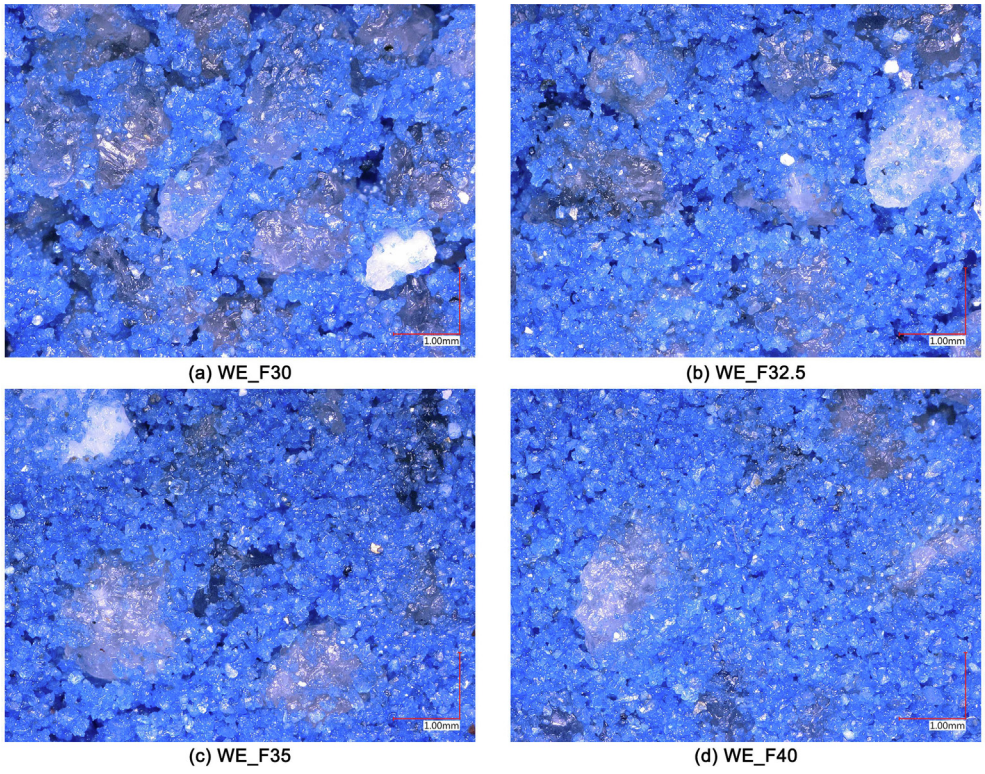

Fig. 4. Microstructure of soils after sample preparation for $FC \geq 30\%$: (a) WE_F30, (b) WE_F32.5, (c) WE_F35, and (d) WE_F40.

the early stage of seepage, but it ceases to increase with time and finally converges to a constant value. This tendency is consistent with the results obtained in relevant studies (Ke and Takahashi, 2014b; Ouyang and Takahashi, 2015). Regarding the evolution of ε_v, it is evident that no significant change in ε_v is observed throughout

Table 3
Summary of major parameters in erosion tests.

Test code	Before-erosion conditions					Onset and end-of-test conditions							Fabric case[b]	Fabric description[c]	Change in k after onset of erosion[d]	Marked volume change	Internal instability phenomenon[e]
	FC	e_c	e_s	D_{rc}	k_i	i_e	m_e	ε_v	FC_e	e_e	e_{se}	k_e					
	(%)			(%)	(m/s)		(%)	(%)	(%)			(m/s)					
WE_F0	0	0.86	0.86	52.5	5.6E−03	–	–	0.01	–	–	–	5.6E−03	–	HS	↕	No	IS
WE_F15	15	0.67	0.96	53.3	5.6E−03	0.15	3.4	0.01	14.6	0.72	1.02	3.9E−03	*i*	UF	↓	No	SF
WE_F20	20	0.61	1.01	53.2	2.0E−03	0.51	1.5	0.02	19.8	0.63	1.04	9.5E−04	*iii*	UF	↓	No	SF
WE_F25	25	0.59	1.12	52.4	4.2E−04	0.86	4.0	0.01	24.2	0.65	1.18	9.4E−04	*iii*	UF	↓↑	No	SF → SU
WE_F30	30	0.55	1.21	52.4	1.9E−04	6.77	0.9	0.01	29.8	0.56	1.22	2.4E−04	*iii* or *iv*	F	↑	No	SU
WE_F32.5	32.5	0.54	1.29	54.2	1.5E−04	11.58	4.7	1.15	31.4	0.60	1.34	7.3E−04	*iv*	OF	↑	Yes	SU → SO
WE_F35[a]	35	0.55	1.38	55.7	1.3E−04	13.18	5.8	0.74	33.7	0.63	1.46	5.7E−04	*iv*	OF	↑	Yes	SO → SF
WE_F40	40	0.58	1.63	53.1	7.7E−05	17.96	3.7	1.04	39.1	0.62	1.66	7.7E−05	*iv*	OF	↕	Yes	IS

Note:
[a] For WE_F35, m_e, ε_v, k_e, and e_e are obtained at $t = 12.8$ min (see Figs. 7 and 11) before the sample failed.
[b] Fabric cases are based on Thevanayagam and Mohan (2000).
[c] CS = host sand, UF = underfilled fabric, F = filled fabric, and OF = overfilled fabric.
[d] ↔ = constant, ↓ = decrease, and ↑ = increase.
[e] SF = self-filtering, SU = suffusion, SO = suffosion, SF = seepage-induced failure, and IS = internal stability.

the test period in this case. This suggests that the structure of the coarse particles does not change with the progress of the erosion of fines. Consequently, the seepage-induced mass loss should directly increase the voids in the sample. Approximately 4.0% of the fines are lost from this sample, yielding $e_e = 0.65$. The determination of e_e will be explained later.

The variations in v and zk with time are shown in Fig. 6c. Before the initiation of erosion, v increases proportionally with i to $i = 0.86$ at about $t = 2.4$ min, yielding an initial permeability of $(k_i) = 4.2 \times 10^{-4}$ m/s. Meanwhile, m_e is observed. After the initiation of erosion, there is a decreased rate of v to $i = 3.68$ at about $t = 4.8$ min, resulting in a decrease in k to 3.1×10^{-4} m/s. Then, an increased rate of v to $i = 6.37$ at $t = 11.0$ min is observed, resulting in an increase in k to 4.1×10^{-4} m/s. After the test reaches a steady state, v gradually increases with a decrease in i until the test is terminated at $t = 44.2$ min, leading to an increase in k to 9.4×10^{-4} m/s. The end-of-test permeability (k_e) is the average value of k for one minute before the no-flow condition, namely, $k_e = 9.4 \times 10^{-4}$ m/s in this case. The temporary decrease in k is attributed to the filtering of the detached fines, leading to partial clogging. k then increases, probably due to a certain preferential flow that can cause the migration of the filtrated particles. The variation in k reflects the complex alteration in seepage during the progression of internal instability; the clogging and migration of the detachable particles during this process induce the heterogeneous variation of the sample. This complex change in permeability is also observed for the gap-graded soil with the initial FC = 25% by Rochim et al. (2017).

The reason why the k of the soil changes during the internal erosion in a micro-scale can be explained through advanced numerical methods with fluid-particle coupling (Nguyen and Indraratna, 2020; Zou et al., 2020). Nguyen and Indraratna (2020) reported that the contact network indicates the strength with which the soil matrix can resist internal erosion and instability because a greater number of contacts among the particles provides greater resistance to the hydraulic force. The total number of particle contacts in the soil does not change until the critical hydraulic force is reached. Afterwards, the particles begin to migrate, leading to a decrease in particle contacts corresponding to an increase in porosity of the sample, which then enhances the permeability.

The seepage response of this test is firstly characterised by constant permeability, followed by a sequence of decreases and increases in permeability, without any change in volumetric strain, accompanied by the migration of fine particles. These responses are referred to as self-filtering; they are followed by suffusion.

4.2. Characterization of seepage-induced internal instability

The time histories of i, k, m_e, and ε_v for all the eroded samples are presented in Fig. 7. In addition, the variation

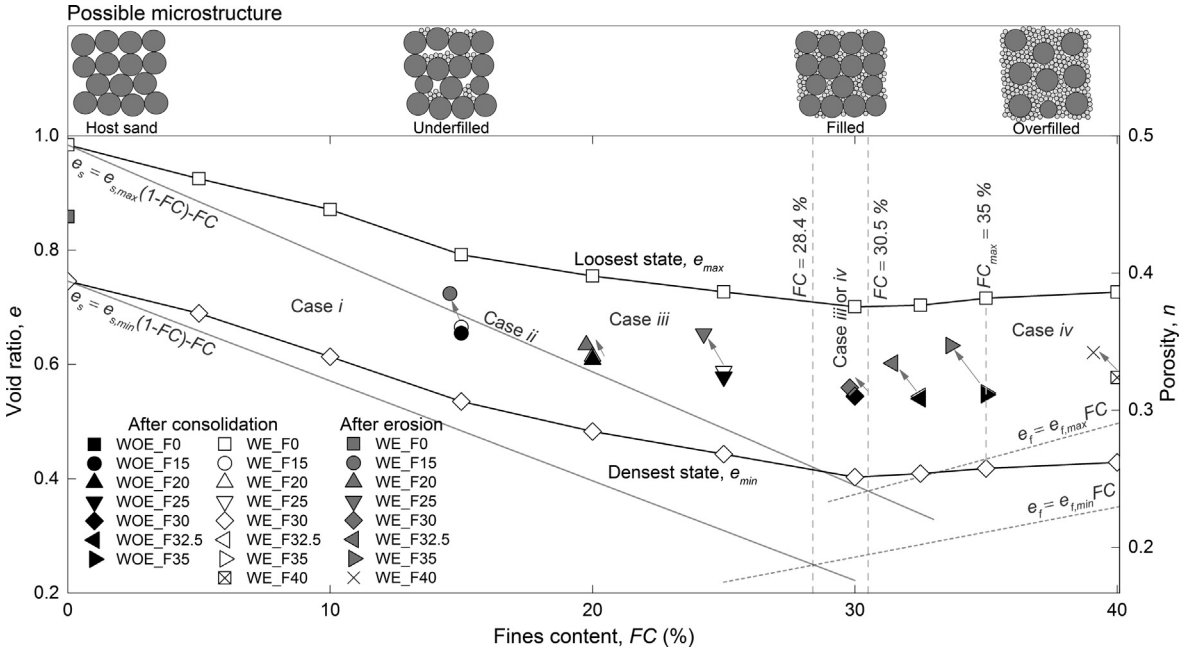

Fig. 5. Identification of initial and post-erosion microstructures of tested soils.

in k plotted against i for each test is shown in Fig. 8. The points at which the increase in m_e is detected are also plotted in both figures. It is revealed that before the initiation of erosion, the variation in k_i does not change with i. k_i is smaller for the sample with the larger FC, which could be attributed to the larger amount of fines, resulting in the more fluid particle-contact area, leading to the larger flow friction and the lower permeability. Nguyen and Indraratna (2017) provited similar evidence of the lower permeability through a micro-analysis of natural fibre composites where different sizes and shapes of fibres were used for the permeability test.

The hydraulic gradient at the initiation of erosion (i_e) is larger for the soil with the larger initial FC, as shown in Table 3. This suggests that the amount of fine particles in the soil has a significant influence not only on the initial permeability, but also on the erosion initiation hydraulic gradient. Moreover, it is noticed that, for the underfilled and filled soils, the initiation of erosion can be identified by the detection of the loss of mass and changes in permeability. For the overfilled soils, on the other hand, the initiation of erosion can be identified not only by the loss of mass and changes in permeability, but also by volumetric strain. A similar observation was made by Slangen and Fannin (2017). They found that the erosion initiation for gradations with $FC = 35\%$ can be detected by changes in permeability and volumetric deformation, while gradations with $FC = 20\%$ can be detected only by changes in permeability.

After the initiation of erosion, the trends for the variations in k, m_e, and ε_v depend on the initial FC and the microstructure type. In the following, the plots in Figs. 7 and 8 and the data in Table 3 are utilised for further characterization of the internal instability according to the terminologies suggested in the literature: self-filtering, suffusion, suffosion, seepage-induced failure, and internally stable state.

4.2.1. Self-filtering

In the underfilled soils, with the initial $FC = 15$ and 20% (WE_F15 and WE_F20), k firstly remains constant at $k_i = 5.6 \times 10^{-3}$ and 2.0×10^{-3} m/s, respectively. After the initiation of erosion at $i_e = 0.15$ and 0.51, the trends are for k to slightly decrease and then to remain constant until the test is terminated, yielding $k_e = 3.9 \times 10^{-3}$ and 9.5×10^{-4} m/s for WE_F15 and WE_F20, respectively. About 3.4% and 1.5% of the fines are lost from the samples without a marked change in ε_v throughout the test for WE_F15 and WE_F20, respectively. The decrease in permeability accompanied by the detection of the loss of fines suggests that some detached particles can become trapped within the soil, which may induce the clogging of the pore throats, leading to a decrease in permeability. The values of the erosion initiation hydraulic gradient obtained for the tested soils show that the underfilled soils with lower fines contents require a relatively smaller hydraulic gradient to initiate the instability process. The instability modes of the samples are characterised by an initial constant permeability followed by a decrease in permeability without marked volumetric deformations. This response is referred to as self-filtering.

4.2.2. Suffusion

In the filled soil with the initial $FC = 30\%$ (WE_F30), k firstly remains constant at $k_i = 1.9 \times 10^{-4}$ m/s. After the initiation of erosion at $i_e = 6.77$, k starts increasing gradually to $k_e = 2.4 \times 10^{-4}$ m/s without a marked change in ε_v; a slight increase to $m_e = 0.9\%$ is observed. The erosion initiation hydraulic gradient appears to be relatively larger in

Table 4
Variation in fine fractions caused by internal erosion.

Test code	Before erosion			After erosion			
	Coarse fraction, W_c (g)	Fine fraction, W_f (g)	Fines content, FC (%)	Eroded fines, ΔW_f (g)	Survived fines, $W_f - \Delta W_f$ (g)	Fines content after erosion, FC_e (%)	Eroded percentage, $m_e = \Delta W_f/W_f$ (%)
WE_F0	941.6	0	0	0	0	0	0
WE_F15	897.3	158.3	15	5.4	152.9	14.6	3.4
WE_F20	867.7	216.9	20	3.3	213.7	19.8	1.5
WE_F25	829.7	276.6	25	11.1	265.4	24.2	4.0
WE_F30	792.1	339.5	30	3.2	336.3	29.8	0.9
WE_F32.5	761.3	366.6	32.5	17.3	349.2	31.4	4.7
WE_F35	728.4	392.2	35	22.7	369.5	33.7	5.8
WE_F40	667.7	445.1	40	16.6	428.6	39.1	3.7

this sample, suggesting that the matrix of fines would be well-connected with greater resistance, which can be driven away by larger hydraulic gradients. Accordingly, the predominant erosion progress in this test is characterised by initial constant permeability and a subsequent increase in permeability without marked volumetric deformation. This response is referred to as suffusion.

4.2.3. Suffosion

In the overfilled soils with the initial $FC = 32.5$, 35, and 40% (WE_F32.5, WE_F35, and WE_F40), the initiation of erosion is found to be $i_e = 11.58$, 13.18, and 17.96, respectively. Before the erosion initiation, the permeability is constant at $k_i = 1.5 \times 10^{-4}$, 1.3×10^{-4}, and 7.7×10^{-5} m/s for WE_F32.5, WE_F35, and WE_F40, respectively. In WE_F32.5, after the erosion initiation, a sudden increase in k is shown along with a marked increase in m_e and a negligible change in ε_v until the test reaches the no-flow condition. Before the test is stopped, significant changes in i and ε_v take place at $t = 43.3$ min (see Fig. 7a and c) that are believed to be the result of localised instability. It is supposed that the structure of the sample does change, due to a significant amount of fines loss, leading to the collapse of the coarse particle packing or the infilling of the void with fine particles. At the end of the test, the permeability increases to $k_e = 7.3 \times 10^{-4}$ m/s, accompanied by $m_e = 4.7\%$ and $\varepsilon_v = 1.15\%$. The instability mode of this sample is characterised by the initial constant permeability, the subsequent noticeable increase in permeability with the absence of a change in volume, and the final subsequent increase in a marked volumetric deformation. In essence, these responses are referred to as suffusion; suffusion is followed by suffosion.

4.2.4. Seepage-induced failure

In WE_F35, after the initiation of erosion at $t = 8.8$ min, the variation in k suddenly increases, corresponding to sharp increases in m_e and ε_v until $t = 12.8$ min, which is indicative of the re-formation of the stable equilibrium of the sample. Thereafter, sharp increases in i, m_e, and ε_v appear, and k suddenly changes (see Fig. 7a–c). At this moment, the test needs to be terminated as the sample has clearly deformed. The pressure control system fails to seek to maintain the target base pressure as a consequence of the equalization between the top and base pressures. The evolutions of axial (from the LVDT) and radial displacements (from RDT#1, RDT#2, and RDT#3) during the erosion process, and the change in the sample profile at the end of erosion, are shown in Fig. 9. The figure indicates that massive deformation occurs mainly in the top half of the sample. It is believed that the water flow will concentrate on a preferential pathway to flush out the fines. The departure of fine particles will create a preferential pore throat or conduit among the coarse particles, along with the sample, and finally lead to soil failure. Due to the failure of the sample, the permeability increases to $k_e = 5.7 \times 10^{-4}$ m/s, accompanied by $m_e = 5.8\%$ and $\varepsilon_v = 0.74\%$. Hence, the instability of this sample is characterised by the initial constant permeability, the subsequent increase in permeability with the contractive volume change, and finally the immediate failure of the sample. These responses are referred to as suffosion; suffosion is followed by seepage-induced failure.

4.2.5. Internally stable state

The test on an internally stable sample with uniform Silica sand No. 3, WE_F0, is conducted to establish a benchmark for a comparative analysis of potentially unstable samples. The seepage test results show that the k of about 5.6×10^{-3} m/s remains constant with no change in ε_v throughout the test. This suggests that there is no change in the microstructure of the sample during the test, yielding an internally stable state.

The test on WE_F40 is conducted to examine the hypothesis that the finer particles completely isolate the coarse particles from other ones at $FC_{max} \geq 35\%$, as proposed by Skempton and Brogan (1994). In this case, the response of the soil to seepage could be internal stability (Shire et al., 2014). It should be noted that WE_F40 is subjected to a maximum of $ITP = 450$ kPa with an attempt to quantify the erosion initiation hydraulic gradient. The seepage test results show that the k of about 7.7×10^{-5} m/s remains constant during the test, suggesting that there is no transportation of soil particles throughout the sam-

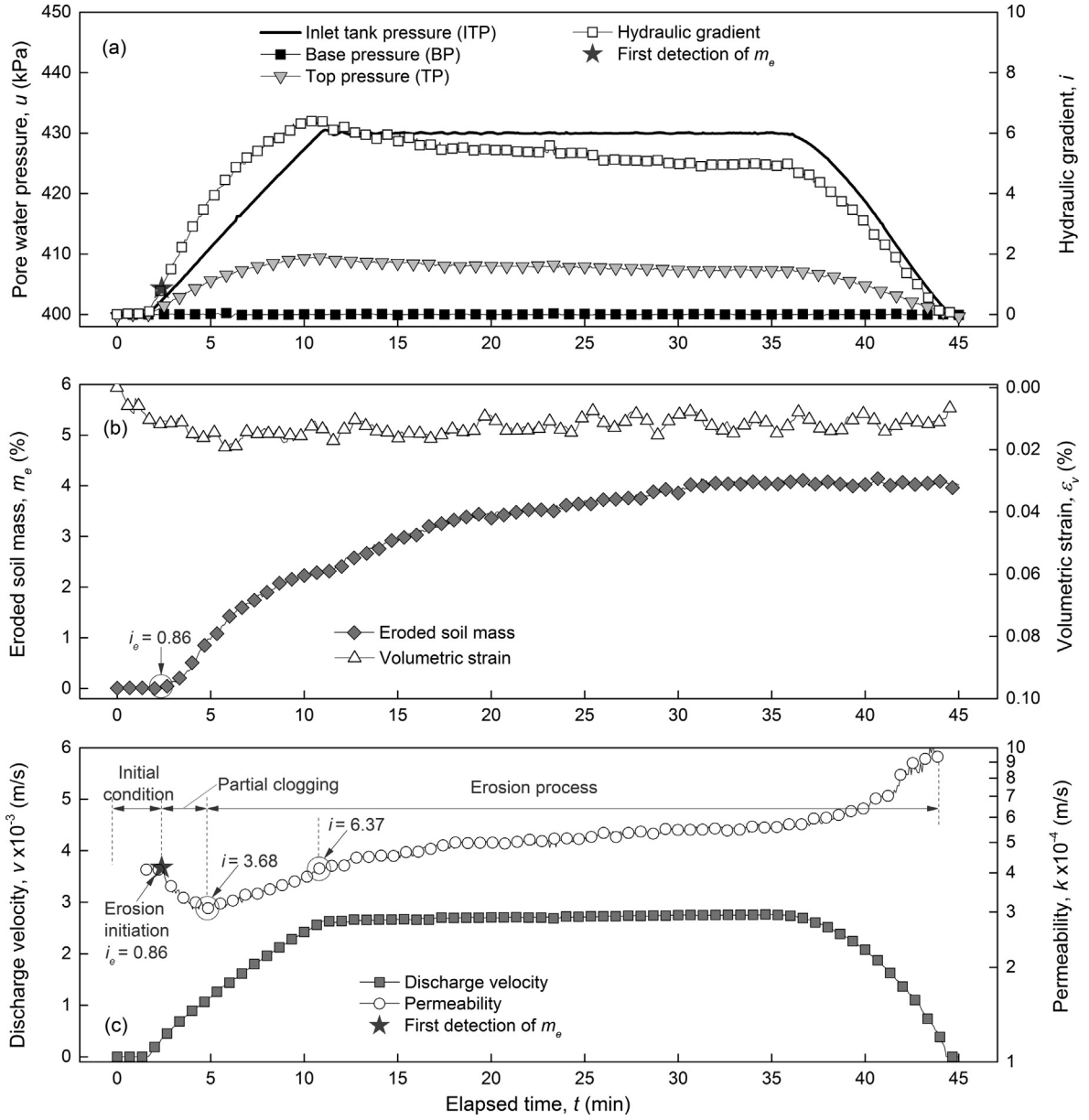

Fig. 6. Typical erosion test results: time histories of (a) pore water pressure and hydraulic gradient, (b) eroded soil mass and volumetric strain, and (c) discharge velocity and permeability for WE_F25.

ple. However, the variation in m_e increases throughout the test, corresponding to ε_v. At the end of the test, $m_e = 3.7\%$ and $\varepsilon_v = 1.04\%$ are recorded. In this sample, since (1) only the radial displacement near the bottom of the sample (RDT #3) is detected and (2) there is no change in permeability, it can be said that the erosion of fines occurs only near the bottom of the sample. Thus, this response is referred to as internal stability.

4.3. Changes in microstructure after internal instability

The occurrences of suffusion (loss of fines with no marked volume change) and suffosion (loss of fines with a marked volume change) alter the microstructure differently. Although a micro-observation has not been performed after the erosion tests, the change in microstructure after erosion could be interpreted only in terms of the change in fines content, global void ratio, and inter-coarse void ratio (Nguyen et al., 2019).

Changes in the global void ratio induced by suffusion and suffosion can be referred to as a variation in the soil phase, as shown in Fig. 10. If suffusion is observed, the total volume of soil remains the same, and the volume of fines loss would be replaced by the same volume of water in a fully saturated condition. The post-suffusion void ratio can be expressed by

$$e_e = \frac{e_c + \left(\Delta W_f / W_f\right)}{1 - \left(\Delta W_f / W_f\right)} \quad \text{for suffosion} \tag{5}$$

where e_c is the void ratio after consolidation, ΔW_f is the cumulative fines loss by mass (equivalent to the volume as the specific gravities of all the particles are the same), and W_f is the initial mass of the fine fraction.

However, if suffosion is observed, the rearrangement of the soil will create a change in the void ratio. Consequently, a volumetric change ($\Delta\varepsilon_v$) occurs and should be added to the void ratio, which is equivalent to $\Delta\varepsilon_v(1 - e_c)$ according to Ke and Takahashi (2014b). The post-suffosion void ratio can be expressed by

$$e_e = (1 - \Delta\varepsilon_v)\left(\frac{e_c + \Delta W_f/W_f}{1 - \Delta W_f/W_f}\right) - \Delta\varepsilon_v \quad \text{for suffosion} \qquad (6)$$

where $\Delta\varepsilon_v$ is the change in volumetric strain due to the erosion process, which is determined from the measured local radial ($\Delta\varepsilon_r$) and axial ($\Delta\varepsilon_a$) strains.

Mitchell (1993) introduced the inter-coarse void ratio (Eq. (1)) as a state variable where the real voids and the volume of the fines are both considered as voids among the coarse particles. As the eroded fines are replaced by the real voids of the coarse particles, the inter-coarse void ratio after erosion (e_{se}) can be expressed by

$$e_{se} = \frac{e_e + FC_e}{1 - FC_e} \qquad (7)$$

$$FC_e = \frac{W_f - \Delta W_f}{W_f - \Delta W_f + W_c} \qquad (8)$$

where e_e is the global void ratio after suffusion or suffosion, FC_e is the fines content by mass after erosion, and W_c is the initial mass of the coarse fraction.

Fig. 11 shows how the e_e and e_{se} vary during the erosion process for the eroded samples. e_e is calculated by Eq. (6) and using data from Table 3, for which the fines loss and volumetric strain in Fig. 7c are used. If there is no volumetric stain, Eq. (6) simply becomes Eq. (5). e_{se} is calculated by Eq. (7) and using data from Table 3. In Fig. 11, the points corresponding to the initiation of erosion (stars) and the onset of the marked volumetric strain (arrows) are also plotted.

For the underfilled and filled samples, $FC \leq FC^*$, and the phenomenon of suffusion is observed (see Fig. 7c). Here, self-filtering is regarded as suffusion since they are both coupled processes (Bonelli, 2012; Rochim et al., 2017). Before erosion, there are no apparent changes in the evolutions of e_e and e_{se} (see Fig. 11), suggesting that there is no change in the soil microstructure. As erosion initiates and progresses, e_e and e_{se} increase due to the erosion of fines. The coarse particles are in contact and may dominate the force chains, as indicated in Fig. 3. Some fines are eroded at low hydraulic gradients as they may be unconnected to the force chains. The fines loss would directly increase the void volume of the coarse particles since there is no sign of particle rearrangement (no volume change) during the erosion process. As a result, the inter-coarse voids become larger and the primary structure formed by the coarse particles will be more unstable.

For the overfilled samples, $FC > FC^*$, and the phenomenon of suffosion is observed (see Fig. 7c). After the onset of erosion, for WE_F35 and WE_F40, e_e and e_{se} increase due to the loss of fines combined with volumetric strain. However, for WE_F32.5, firstly, e_e and e_{se} gradually increase due to the loss of fines, and then sharp drops in e_e and e_{se} appear at $t = 43.3$ min, as a consequence of the marked volume change (see Fig. 11). These drops in the void ratios might be related to the rearrangement of the coarse particle packing, which may have locally occurred somewhere inside the sample. The fines matrix disperses the coarse particles, as indicated in Fig. 4, and provides the main supports to the force chains as they can be eroded at high hydraulic gradients. Their loss weakens and/or removes the supports, leading to the sudden buckling of the force chains through the coarse particles; consequently, a sudden volumetric contraction may occur. This buckling leads to the coarse particles rearranging themselves into a new equilibrium with better contacts; consequently, the inter-coarse voids may decrease. However, more microstructural observations during the erosion process will be necessary in order to confirm these hypotheses.

Fig. 5 shows the FC_e and e_e at the end of erosion of the eroded samples and the FC and e of the non-eroded samples. In general, the state point moves toward the loosest state line, suggesting that the eroded samples become weaker after erosion. However, suffusion (loss of fines with no marked volume change) and suffosion (loss of fines with a marked volume change) might affect the mechanical behaviour differently. The next section demonstrates the impact of internal erosion on the undrained mechanical response of soils during shearing.

5. Undrained mechanical response in triaxial compression

Figs. 12 and 13 show deviator stress (q) versus axial strain (ε_a), pore water pressure (u) versus axial strain, and deviator stress versus mean effective stress (p') or effective stress path for the undrained compression tests on the non-eroded and eroded specimens ($q = [\sigma'_a - \sigma'_r]/2$ and $p' = [\sigma'_a + 2\sigma'_r]/3$ where σ'_a is the effective axial stress and σ'_r is the effective radial stress). The global void ratio, inter-coarse void ratio, fines content before compression, and instability phenomenon are also denoted in the figures. A summary of the test results is presented in Table 5.

5.1. Effects of fines content on mechanical response of non-eroded samples

The effective stress paths of WOE_F0, WOE_F15, and WOE_F20 exhibit dilative behaviour (i.e., the samples develop large negative pore water pressure). As a result, the mean effective stress continuously increases even after passing through the phase transformation state. In contrast, the effective stress paths of WOE_F25 exhibit contractive-dilative behaviour (i.e., the pore water pressure firstly decreases and then increases). The peak strength of

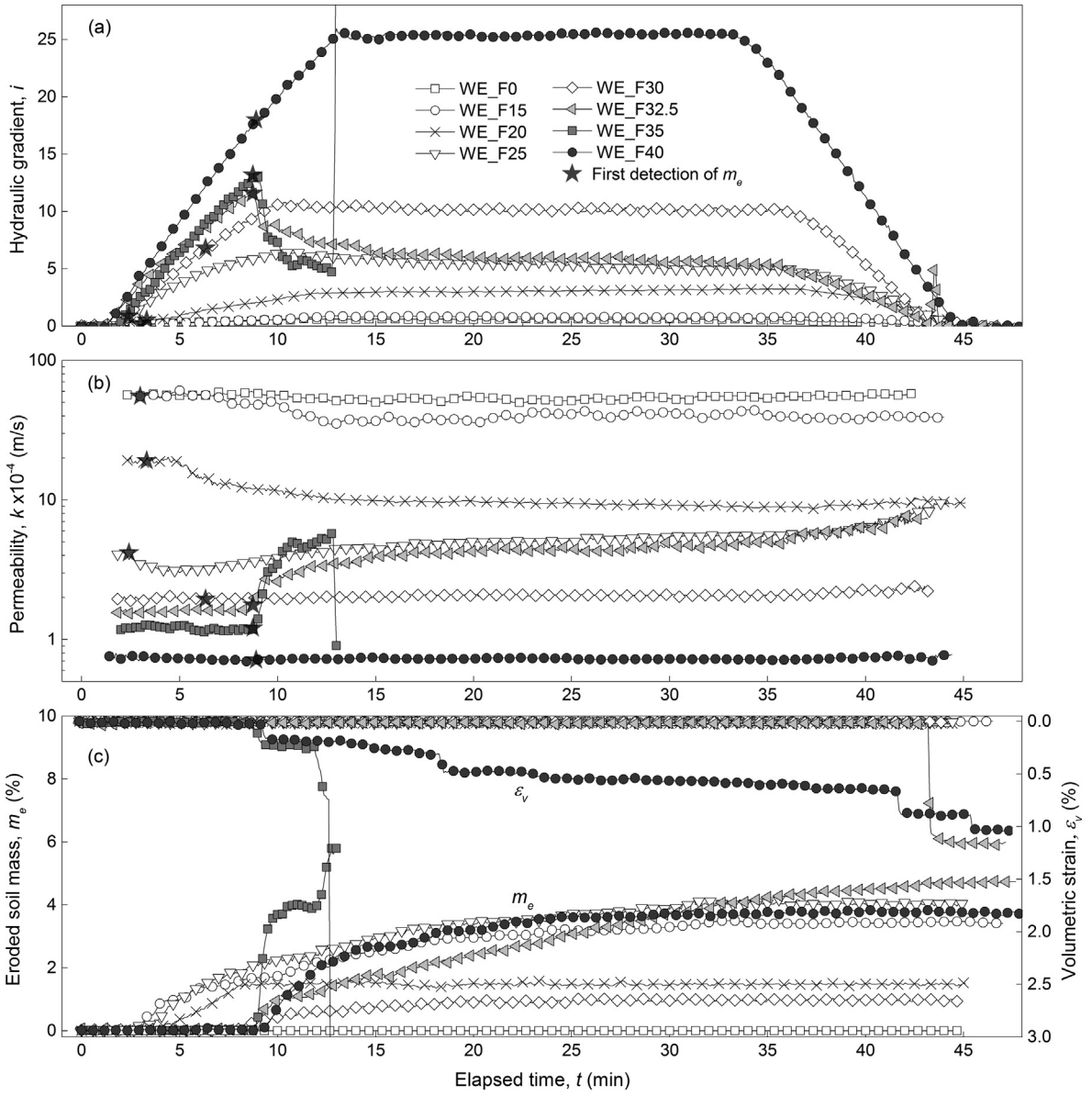

Fig. 7. Time histories of (a) hydraulic gradient, (b) permeability, and (c) eroded soil mass and volumetric strain for all eroded samples.

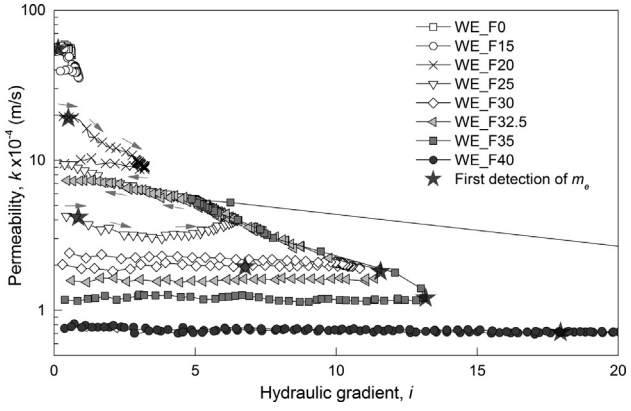

Fig. 8. Relationship between permeability and hydraulic gradient.

the samples is smaller than for WOE_F0 or WOE_F15 even though e_c is smaller. In these cases, the stress-strain curves show the peak followed by strain-softening. Then, the deviator stress starts increasing again with straining due to dilative behaviour after passing through the phase transformation point. The change in mechanical behaviour can be attributed to the lubrication of the contacts among the coarse particles induced by the fine particles during shearing. The test on the host sand (Silica sand No. 3 alone) shows the highest strength and dilative behaviour throughout compression as the particles are fully in contact with each other and dominate the stress transfer. The stress–strain response is fully characterized by the interlocking among the coarse particles. With an increase in the fines content, some fines may lie within the inter-

coarse voids, while some of them may separate the coarse particles. The separators may produce lubrication that lessens the resistance against the coarse particle movement during shearing, resulting in larger compressibility. Continuous shearing may bring about the rearrangement of the coarse particles, resulting in better contact and leading to dilative behaviour at larger axial strain levels.

With a further increase in fines to 30%, WOE_F30 starts showing contractive behaviour (i.e., positive pore water pressure) and smaller shear strength. As the fines content is increased even further to 32.5% and 35% (WOE_F32.5 and WOE_F35), the samples become more contractive (i.e., the pore water pressure develops more quickly) and show less shear strength. Most of the coarse particles may be isolated by the fine particles or floating in the matrix of fines. The contractive stress–strain behaviour will mainly be dominated by the compressibility of the fines matrix. In summary, for the non-eroded samples, the shear strength generally decreases, and the soil becomes more contractive with an increase in *FC*. These results agree with previous investigations (*e.g.*, Yamamuro and Lade, 1997; Thevanayagam and Mohan, 2000; Thevanayagam et al., 2002; Ke and Takahashi, 2015).

5.2. Effects of loss of fines on mechanical response of eroded samples

Fig. 12a–c show the stress-strain curves, pore water pressure, and effective stress paths of the host sand sample (WOE_F0) and the samples with the initial $FC = 15\%$ (WOE_F15 and WE_F15). It is seen that the shear strength of WOE_F15 and WE_F15 is smaller than that of WOE_F0, although the global void ratios are smaller. This can be attributed to the lubrication of the coarse particle contacts induced by the fines during shearing, as discussed in the previous section. Comparing WE_F15 to WOE_F15, although the internal erosion does make the e_e value of WE_F15 larger than the e_c value of WOE_F15, no significant change in the stress-strain curve or the effective stress path is observed in WE_F15. Moreover, the effective stress paths of these samples are similar to those of the host sand sample (WOE_F0). Before erosion, the $e_c - FC$ relation of WE_F15 is Case *i* by Thevanayagam and Mohan (2000), as shown in Fig. 5, where e_s is smaller than the maximum inter-coarse void ratio ($e_{s,\max} = 0.98$). The same is true for WOE_F15. In this case, the coarse particles are in contact, on average, forming inter-coarse voids; some fines may sit loosely in the voids. Therefore, the stress–strain responses are mainly derived from friction along with the coarse particle contacts, although the e_{se} of WE_F15 is larger than $e_{s,\max}$ after erosion. The increase in the inter-coarse void ratio is likely to be due to the loss of loose fines in the voids. This result also suggests that the strength characteristics of the soil will be unaffected by the erosion of fines in this range of *FC*.

For samples with the initial *FC* of 20, 25, and 30%, the eroded samples show smaller peak deviator stress, a larger degree of strain softening, and a more contractive response, as shown in Figs. 12d–f, 13a–c, respectively. Interestingly, sudden drops in deviator stress accompanied by sharp increases in pore water pressure and radial strains are detected before the peak at the small strain level for some of the post-suffusion samples (WE_F25 and WE_F30), as shown in Fig. 14. These responses are caused by the increase in inter-coarse voids due to the loss of fines without the rearrangement of the coarse particles. Consequently, the unstable or collapsible structure of the coarse particles is created. Upon shearing, a sudden collapse of the structure will occur instantly, leading to smaller and sudden drops in shear strength. These results suggest that suffusion strongly affects the strength characteristics of soil having the initial *FC* in a range of 20–30%, although the observed amount of fines loss is small. However, the effect of the spatial distribution of the survived fines induces heterogeneity in the microstructure of the soils, as demonstrated by Nguyen et al. (2019), and can affect the post-erosion mechanical test. Further investigation of this aspect is necessary.

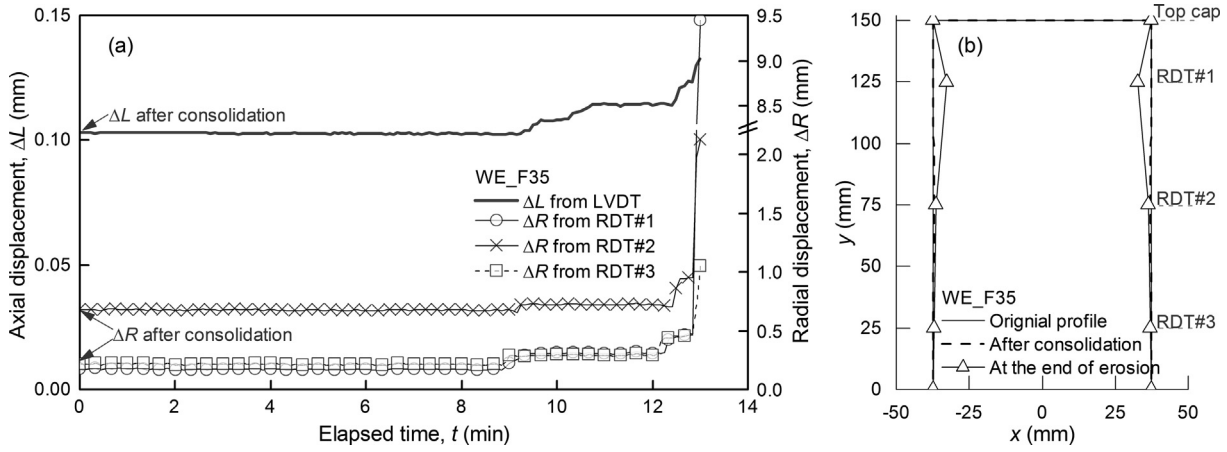

Fig. 9. Changes in (a) axial and radial displacements during erosion process, and (b) sample profile at end of erosion for WE_F35.

For the sample with the initial $FC = 32.5\%$, the post-suffosion sample, WE_F32.5, shows smaller peak deviator stress and a more dilative tendency at a large strain level, as shown in Fig. 13c–e. The smaller strength of WE_F32.5 is due to the larger void ratios after erosion, while the more dilative behaviour at a large strain level is caused by the particle rearrangement induced by the collapse of the coarse particle packing or the infilling of the inter-coarse voids with fines.

6. Discussions

6.1. Influence of fines on initiation and progress of internal instability

Internal instability phenomena have been reported differently by many researchers in terms of permeability and volume change. Chang and Zhang (2011), for example, used the gap-graded soil with the initial $FC = 35\%$ and noted that the permeability increased and reached a constant value with contractive volume changes during the development of erosion. Xiao and Shwiyhat (2012) noted that the permeability decreased with volume changes due to erosion and the subsequent clogging of fines in all gap-graded soils with the initial $FC = 16$, 30, and 50%. Rochim et al. (2017) reported that the hydraulic loading history influenced the occurrence of self-filtering or erosion. In this study, the erosion test results indicate that, under the same hydraulic loading, the instability phenomena are significantly affected by the microstructure in the soil mixture. Depending on the initial fines content, the gap-graded soils show self-filtering, suffusion, suffosion, seepage-induced failure, or internally stable state. Fig. 15 shows the internal instability identification diagram, in terms of the void ratio and fines content, to summarise the initiation and progress of the internal instability phenomena and the possible microstructures.

When $FC < FC^*$, the soil microstructure is "underfilled"; fine particles are confined within the voids between the coarse particles. The phenomena of self-filtering and

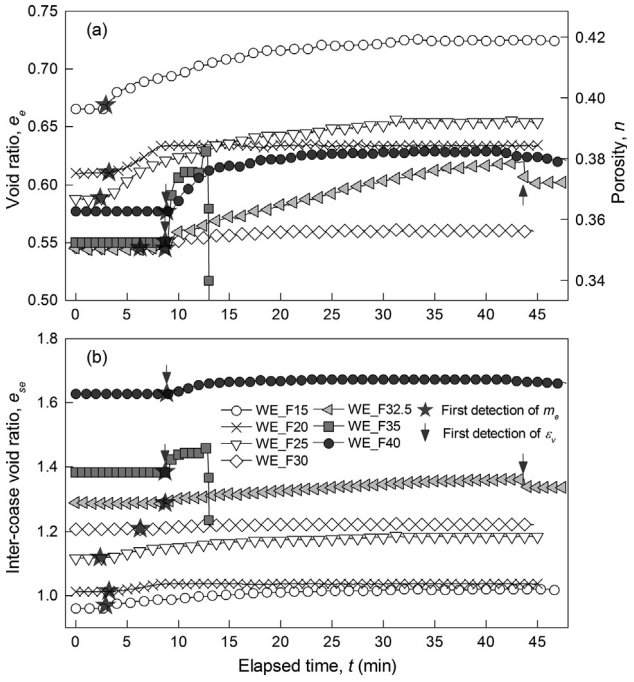

Fig. 11. Evolutions of (a) void ratio and (b) inter-coarse void ratio.

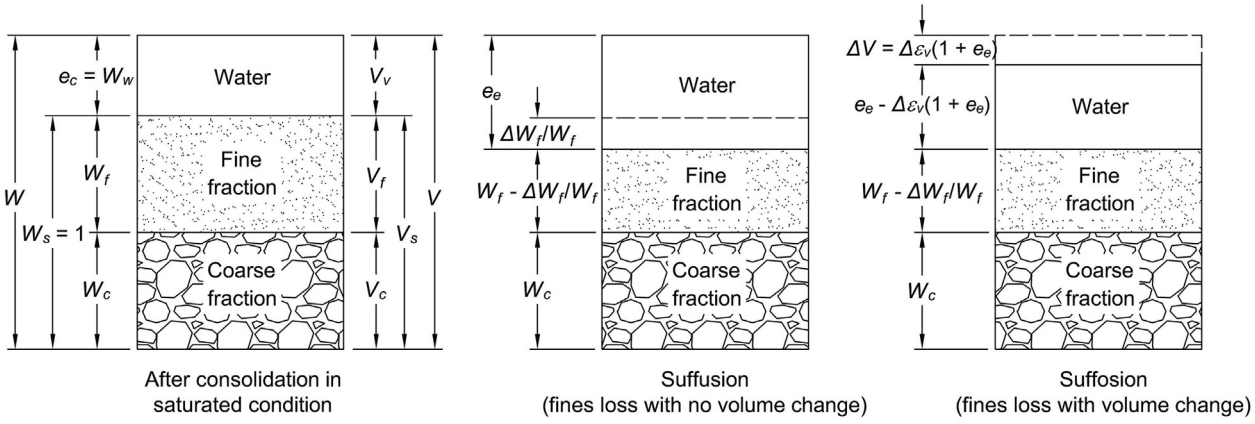

Fig. 10. Variation in soil phase induced by suffusion and suffosion.

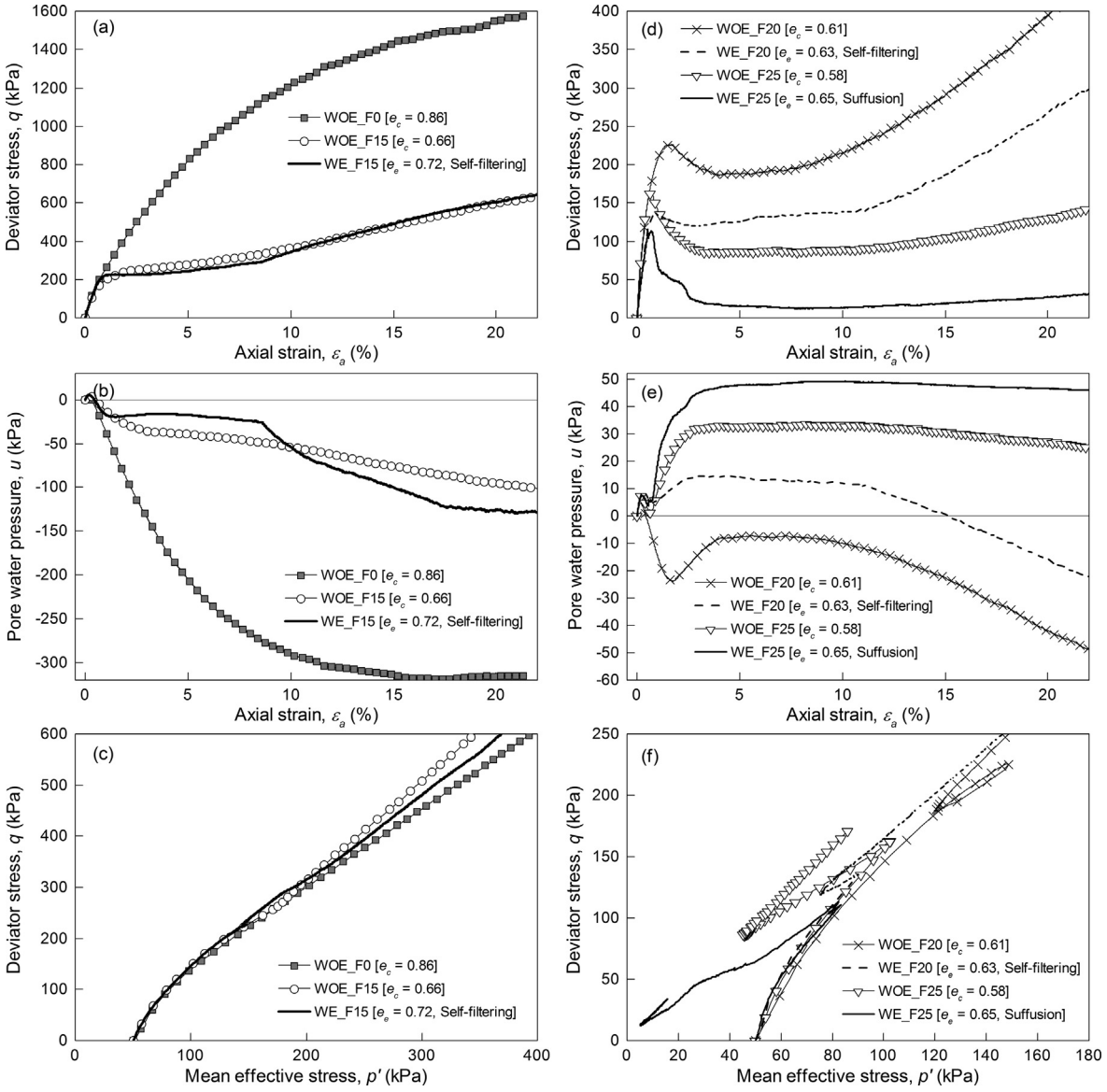

Fig. 12. Undrained compression test results for samples with $FC < 30\%$.

suffusion are evident in this type of soil. The fine particles can migrate or be trapped in the sample without the loss of matrix integrity at a relatively small hydraulic gradient. If the hydraulic gradient exceeds a certain value, the suspended fines will be eroded out. When $FC \approx FC^*$, the soil microstructure is "filled"; it is hypothesised that both coarse and fine particles contribute to the soil matrix and that the amount of fine particles is sufficient for contact to be made among the particles and for the particles to be packed tightly in the voids formed by the coarse particles. In this case, suffusion can occur, but would require a relatively large hydraulic gradient for the fine particles to migrate. When $FC > FC^*$, the soil microstructure is "overfilled"; a matrix of fines disperses the coarse particles. The fine particles play a major role in the stress-transfer, while the coarse particles make a minor contribution. A relatively large hydraulic gradient would be required to demolish the matrix of fines. This type of soil could be vulnerable to suffosion (*e.g.*, WE_F32.5) or seepage-induced failure (*e.g.*, WE_F35). When $FC > 35\%$, which is larger than the limit of $FC_{max} = 35\%$ given by Skempton and Brogan (1994) (*e.g.*, WE_F40), the coarse particles are completely dispersed by fines, leading to an internally stable state.

It should be noted that the diagram in Fig. 15 can be used to gain a rough idea of what might be expected for freshly compacted, non-plastic, gap-graded sands. The effects of ageing, cementation, etc. are not considered in this study. Moreover, the effects of the hydraulic loading history, relative density, confining effective stress, and filter ratio (D_{15c}/D_{85f}) on the initiation and progress of internal instability must also be taken into consideration.

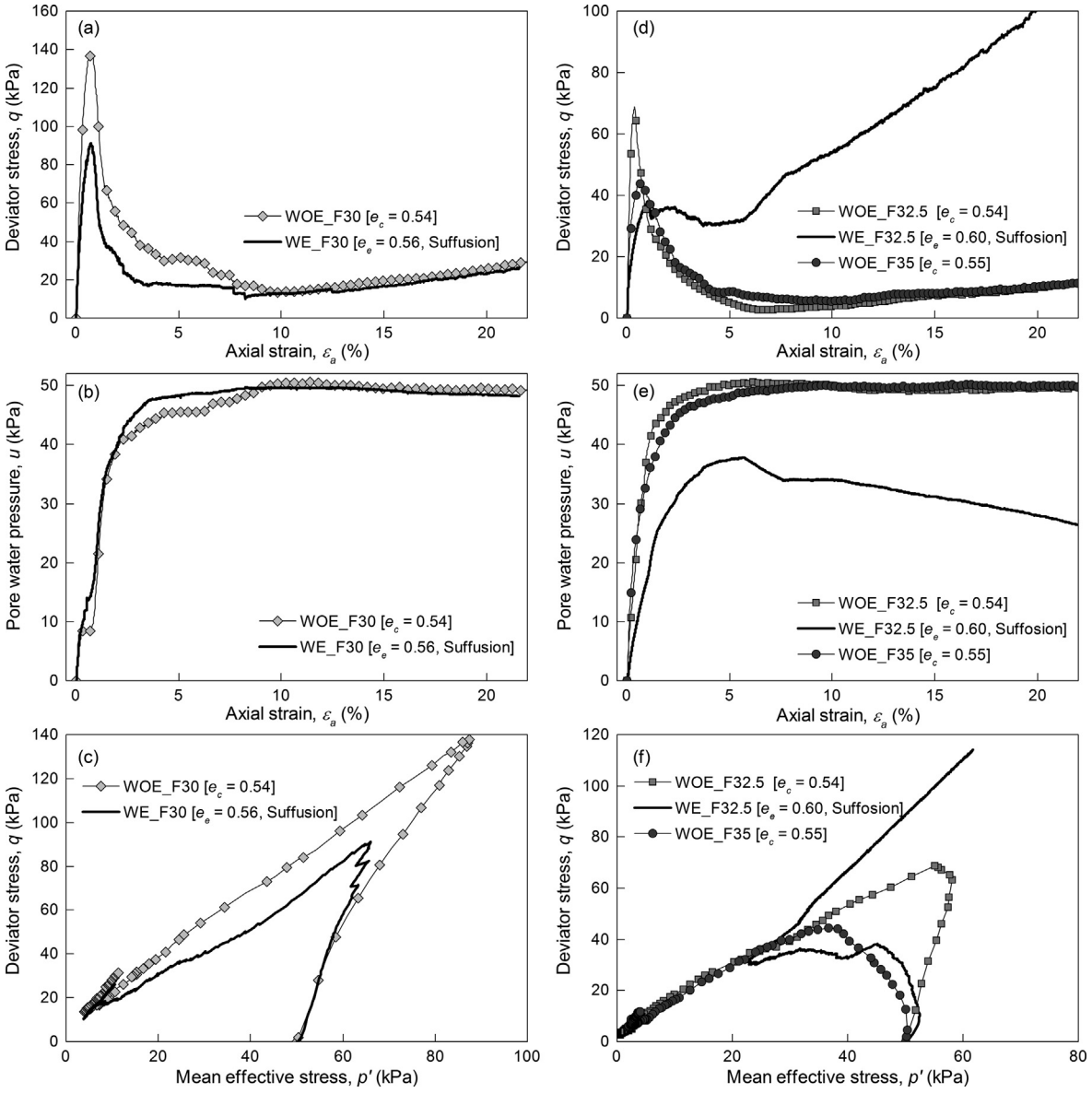

Fig. 13. Undrained compression test results for samples with $FC \geq 30\%$.

Table 5
Summary of main parameters in undrained compression tests.

Test code	FC or FC_e (%)	e_c or e_e	e_s or e_{se}	q_p (kPa)	q_{ss} (kPa)	Fabric case	Fabric description	Stress-strain behaviour[a]
WOE_F0	0	0.86	0.86	–	–	–	HS	D
WOE_F15	15	0.66	0.95	–	–	*i*	UF	D
WOE_F20	20	0.61	1.01	226.0	186.0	*iii*	UF	D
WOE_F25	25	0.58	1.10	162.9	85.4	*iii*	UF	C–D
WOE_F30	30	0.54	1.21	137.7	13.6	*iii* or *iv*	F	C
WOE_F32.5	32.5	0.54	1.28	68.8	2.5	*iv*	OF	C
WOE_F35	35	0.55	1.38	44.8	5.4	*iv*	OF	C
WE_F15	14.6	0.72	1.02	–	–	*iii*	UF	D
WE_F20	19.8	0.63	1.04	136.8	118.4	*iii*	UF	C–D
WE_F25	24.2	0.65	1.18	112.4	11.9	*iii*	UF	C
WE_F30	29.8	0.56	1.22	91.1	10.1	*iii* or *iv*	F	C
WE_F32.5	31.4	0.60	1.34	38.2	30.1	*iv*	OF	C–D

Note: [a]D = dilative, C = contractive, and C–D = contractive followed by dilative.

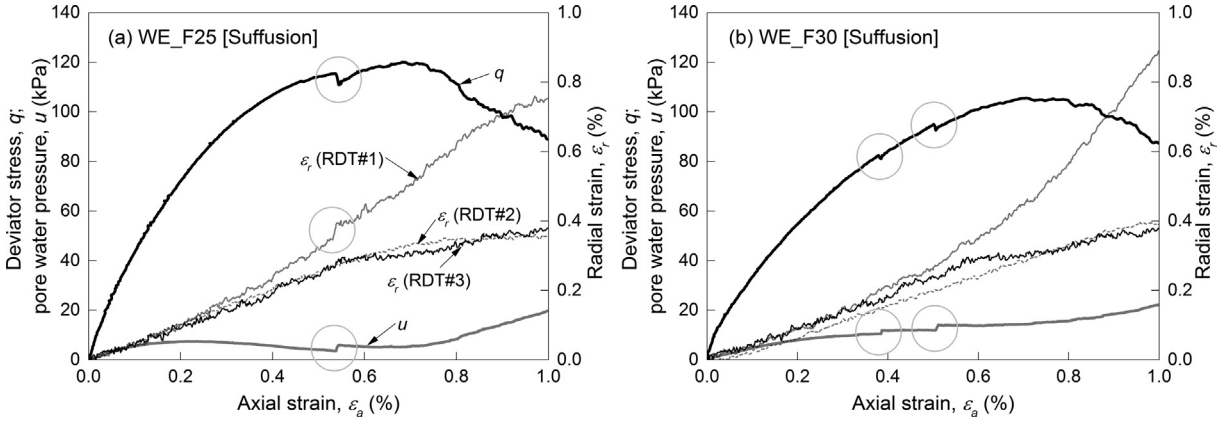

Fig. 14. Changes in deviator stress, pore water pressure, and radial strain against axial strain at small axial strain level: (a) WE_F25 and (b) WE_F30.

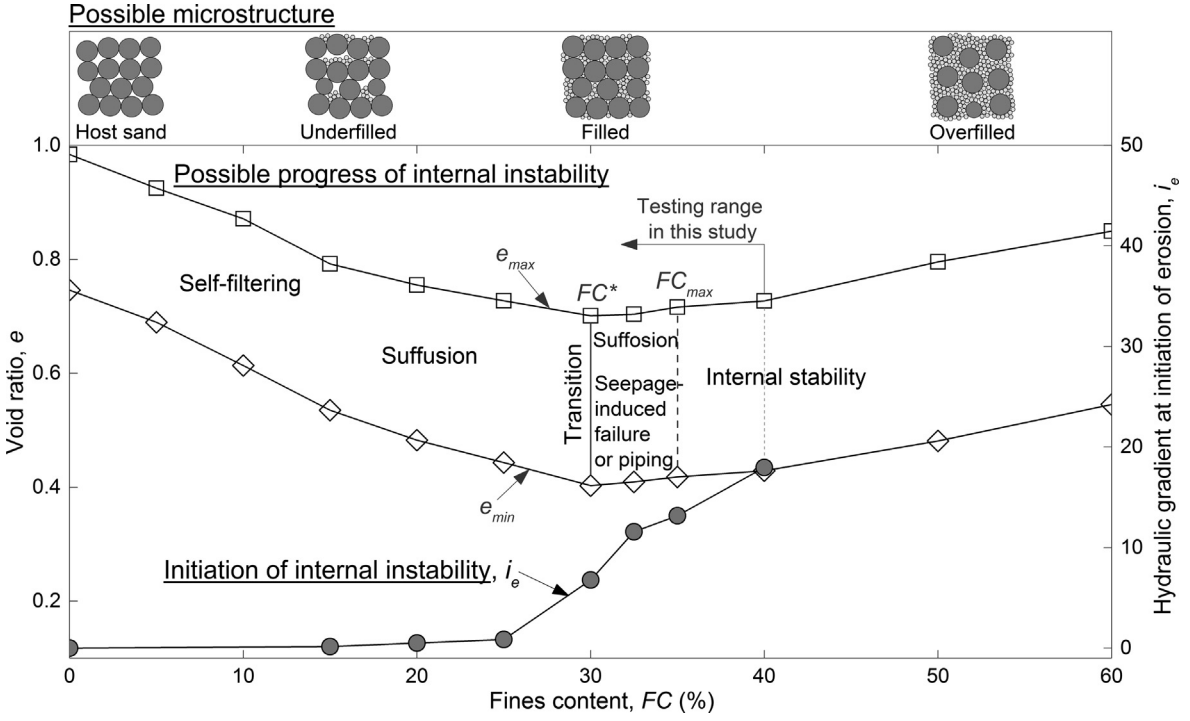

Fig. 15. Diagram of internal instability identification for void ratio versus fines content and possible gap-graded soil microstructure.

6.2. Impact of internal instabilities on undrained mechanical response

The impact of internal instability on the undrained mechanical responses given in literature has shown results contradictory to those expected (Xiao and Shwiyhat, 2012; Ke and Takahashi, 2014b; Ouyang and Takahashi, 2015; Mehdizadeh et al., 2017). For instance, Ke and Takahashi (2014b) and Ouyang and Takahashi (2015) conducted undrained compression tests on eroded gap-graded soils and found that the shear strength was larger than those of non-eroded soils. The soils became more dilative after erosion. They suggested that the coarser particles suffered from significant redisposition during seepage, resulting in a marked volumetric strain. The seepage response matched the mode of suffosion (Fannin & Slangen, 2014).

In this study, the undrained compression test results indicate that the alteration in the undrained mechanical response depends on the occurrence of internal instability phenomena and the fines content. For the soils with small initial fines contents (*e.g.*, WE_15), the mechanical response might be unaffected by internal instability due

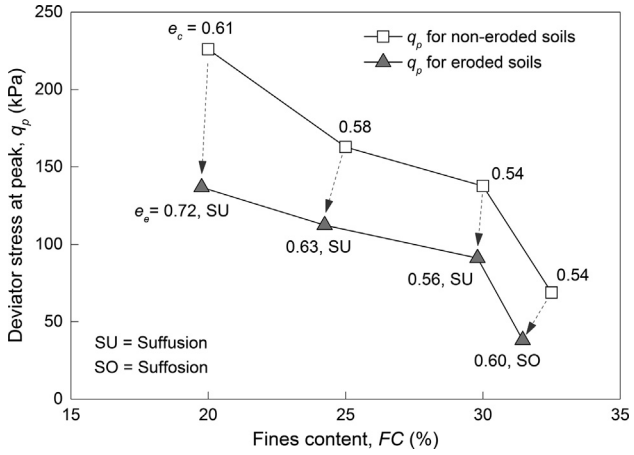

Fig. 16. Deviator stress at peak versus fines content.

to the coarse-dominated microstructure, as shown in Fig. 12. Fig. 16 shows the variation in peak deviator stress (q_p) with the fines content before shearing (FC or FC_e). The void ratios before shearing (e_c or e_e) are also shown in the figure. The q_p significantly decreases with an erosion-induced increase in the void ratio. The increase in the void ratio induced by the fines loss might be an indicator for evaluating the post-erosion mechanical behaviour. The results suggest that if suffusion (fines loss without volume change) happens to soils having the initial FC of about 20–30% (*e.g.*, WE_20, WE_25, and WE_30), the mechanical response will be significantly affected by the loss of fines without a change in the coarse particle packing. In this case, the soil strength dramatically decreases and becomes more contractive, although the amount of erosion is small, as shown in Fig. 12. Due to the localised small collapse, sudden drops in deviator stress and sharp increases in pore water pressure or radial strain with axial straining are detected at small strain levels, as shown in Fig. 14. This might be an indication of the deterioration of the unstable soil packing.

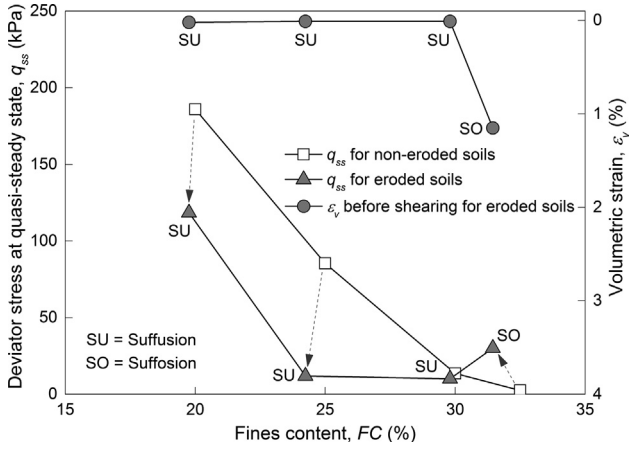

Fig. 17. Deviator stress at quasi-steady state and volumetric strain before shearing versus fines content.

Fig. 17 shows the deviator stress at the quasi-steady stage (q_{ss}) versus FC or FC_e together with ε_v before shearing for eroded samples. The q_{ss} decreases for soils experiencing suffusion; a drastic decrease is especially observed at the FC of about 20–25%. If the soil experiences suffosion (fines loss with a marked volume change) (*e.g.*, WE_32.5), the stress-strain curve of the soil will become more dilative and show larger shear stress at large strain levels, as shown in Fig. 13. This is likely to be due to the soil rearrangement before shearing, as reported in the literature.

For engineering purposes, the fines content of about 20–30% may be used as a discrimination range of fines contents in order to recognise the suffusion phenomenon. Under such a condition, the fine particles can be eroded at small hydraulic gradients without altering the soil structure, resulting in a change in permeability and a significant decrease in the post-suffusion shear strength. Moreover, the decrease in shear strength also suggests that suffusion will be a serious concern in the long-term stability of earth structures. Immediate rehabilitation of the earth structure showing signs of suffusion may be necessary.

7. Conclusions

A series of experiments was carried out to investigate the influence of fines on the initiation and progress of the seepage-induced internal instability of gap-graded sands and its impact on the undrained mechanical response. A pressure-controlled triaxial erosion system was used in this study. Tests on gap-graded sands with various fines contents were conducted. The soils were compressed by undrained monotonic compression to observe the impact of internal instability on the soil responses. Based on the experimental results, the following conclusions can be drawn:

- The proposed internal instability identification diagram (Fig. 15) can help to categorise the initiation and progress of the instability phenomena of gap-graded sands. With small fines contents ($FC < FC^*$), the soil is susceptible to self-filtering or suffusion, which can be initiated at relatively small hydraulic gradients due to a coarse-dominated microstructure. With transitional fines contents ($FC \approx FC^*$), the soil is susceptible to suffusion, which can be initiated at relatively high hydraulic gradients. With large fines contents ($FC > FC^*$), the soil is susceptible to suffosion, seepage-induced failure, or an internally stable state, depending on the amount of initial fines that contributes to the soil microstructure. The instabilities can be initiated at large hydraulic gradients in this case.
- When suffusion occurs, seepage-induced mass loss without a significant volume change, accompanied by an increase of permeability, is observed. Seepage-induced suffusion significantly affects the undrained mechanical behaviour of the soils. The soils become looser because of the loss of fines without a volume change. The eroded

samples were seen to have smaller shear strength and to show a more contractive response than the non-eroded samples, although the amount of eroded soil mass was small.

- Suffusion may create an unstable structure in the soils. Due to a localised small collapse, sudden drops in deviator stress and sharp increases in pore water pressure and radial strain with axial straining were detected in the eroded samples at small strain levels, which are regarded as evidence of the soil becoming collapsible due to deterioration.
- When suffosion occurs, seepage-induced mass loss accompanied by a reduction in volume is observed. In this study, the undrained mechanical response of the soil showed a more dilative tendency at large strain levels due to the rearrangement of the soil.

Acknowledgements

The first author would like to acknowledge the scholarship support of the Japanese Government (Monbukagakusho: MEXT). This work was partially supported by JSPS KAKENHI Grant No. 19H02232.

References

Altuhafi, F., O'Sullivan, C., Cavarretta, I., 2013. Analysis of an image-based method to quantify the size and shape of sand particles. J. Geotech. Geoenviron. Eng. 139 (8), 1290–1307.

ASTM D2487-11, 2012. Standard practice for classification of soils for engineering purposes (Unified Soil Classification System). Annual Book of ASTM Standards. ASTM International, West Conshohocken, PA.

ASTM E2655-08, 2008. Standard guide for reporting uncertainty of test results and use of the term measurement uncertainty in ASTM test methods. Annual Book of ASTM Standards. ASTM International, West Conshohocken, PA.

Bendahmane, F., Marot, D., Alexis, A., 2008. Experimental parametric study of suffusion and backward erosion. J. Geotech. Geoenviron. Eng. 134 (1), 57–67.

Bonelli, S., 2012. Erosion of Geomaterials. John Wiley & Sons.

Chang, D.S., Zhang, L.M., 2011. A stress-controlled erosion apparatus for studying internal erosion in soils. Geotech. Test. J. 34 (6), 579–589.

Chang, D.S., Zhang, L.M., 2012. Critical hydraulic gradients of internal erosion under complex stress states. J. Geotech. Geoenviron. Eng. 139 (9), 1454–1467.

Fannin, R.J., Slangen, P., 2014. On the distinct phenomena of suffusion and suffosion. Géotechnique Lett. 4 (4), 289–294.

Fell, R., Wan, C.F., Cyganiewicz, J., Foster, M., 2003. Time for development of internal erosion and piping in embankment dams. J. Geotech. Geoenviron. Eng. 129 (4), 307–314.

International Commission on Large Dams (ICOLD), 2013. Bulletin on internal erosion of dams, dikes and their foundations.

Jiang, M.J., Konrad, J.M., Leroueil, S., 2003. An efficient technique for generating homogeneous samples for DEM studies. Comput. Geotech. 30 (7), 579–597.

Ke, L., Takahashi, A., 2012. Strength reduction of cohesionless soil due to internal erosion induced by one-dimensional upward seepage flow. Soils Found. 52 (4), 698–711.

Ke, L., Takahashi, A., 2014a. Triaxial erosion test for evaluation of mechanical consequences of internal erosion. Geotech. Test. J. 37 (2), 347–364.

Ke, L., Takahashi, A., 2014b. Experimental investigations on suffusion characteristics and its mechanical consequences on saturated cohesionless soil. Soils Found. 54 (4), 713–730.

Ke, L., Takahashi, A., 2015. Drained monotonic responses of suffusional cohesionless soils. J. Geotech. Geoenviron. Eng. 141 (8), 04015033.

Kenney, T.C., Lau, D., 1985. Internal stability of granular filters. Can. Geotech. J. 23 (3), 420–423.

Kenney, T.C., Lau, D., 1986. Internal stability of granular filters: Reply. Can. Geotech. J. 23 (3), 420–423.

Kézdi, A., 1979. Soil Physics: Selected Topics. Elsevier Scientific Publishing Co., Amsterdam.

Ladd, R.S., 1978. Preparing test specimens using undercompaction. Geotech. Test. J. 1 (1), 16–23.

Lade, P.V., Liggio, C.D., Yamamuro, J.A., 1998. Effects of non-plastic fines on minimum and maximum void ratios of sand. Geotech. Test. J. 21, 336–347.

Li, M., Fannin, R.J., 2008. Comparison of two criteria for internal stability of granular soil. Can. Geotech. J. 45 (9), 1303–1309.

Marot, D., Bendahmane, F., Rosquoet, F., Alexis, A., 2009. Internal flow effects on isotropic confined sand-clay mixtures. Soil Sediment Contam. 18 (3), 294–306.

Mehdizadeh, A., Disfani, M.M., Evans, R., Arulrajah, A., 2017. Progressive internal erosion in a gap-graded internally unstable soil: mechanical and geometrical effects. Int. J. Geomech. 18 (3), 04017160.

Mitchell, J.K., 1993. Fundamentals of Soil Behavior. John Wiley & Sons, New York, pp. 1–210.

Moffat, R., Fannin, R.J., 2011. A hydromechanical relation governing internal stability of cohesionless soil. Can. Geotech. J. 48 (3), 413–424.

Moffat, R., Fannin, R.J., Garner, S.J., 2011. Spatial and temporal progression of internal erosion in cohesionless soil. Can. Geotech. J. 48 (3), 399–412.

Muir Wood, D., 2007. The magic of sands—the 20th Bjerrum Lecture presented in Oslo, 25 November 2005. Can. Geotech. J. 44 (11), 1329–1350.

Nguyen, C.D., Benahmed, N., Andò, E., Sibille, L., Philippe, P., 2019. Experimental investigation of microstructural changes in soils eroded by suffusion using X-ray tomography. Acta Geotech. 14 (3), 749–765.

Nguyen, T.T., Indraratna, B., 2017. Experimental and numerical investigations into hydraulic behaviour of coir fibre drain. Can. Geotech. J. 54 (1), 75–87.

Nguyen, T.T., Indraratna, B., 2020. A coupled CFD–DEM approach to examine the hydraulic critical state of soil under increasing hydraulic gradient. Int. J. Geomech. 20 (9), 04020138.

Ouyang, M., Takahashi, A., 2015. Influence of initial fines content on fabric of soils subjected to internal erosion. Can. Geotech. J. 53, 299–313.

Pachideh, V., Hosseini, S.M.M.M., 2019. A new physical model for studying flow direction and other influencing parameters on the internal erosion of soils. Geotech. Test. J. 42 (6), 1431–1456.

Peng, M., Zhang, L.M., 2012. Breaching parameters of landslide dams. Landslides 9 (1), 13–31.

Powers, M.C., 1953. A new roundness scale for sedimentary particles. J. Sediment. Res. 23 (2), 117–119.

Razavi, S.K., Hajialilue Bonab, M., Dabaghian, A., 2020. Investigation into the internal erosion and local settlement of Esfarayen earth-fill dam. J. Geotech. Geoenviron. Eng. 146 (4), 04020006.

Reddi, L.N., Lee, I.M., Bonala, M.V.S., 2000. Comparison of internal and surface erosion using flow pump tests on a sand-kaolinite mixture. Geotech. Test. J. 23 (1), 116–122.

Rochim, A., Marot, D., Sibille, L., Thao Le, V., 2017. Effects of hydraulic loading history on suffusion susceptibility of cohesionless soils. J. Geotech. Geoenviron. Eng. 143 (7), 04017025.

Shire, T., O'Sullivan, C., Hanley, K.J., 2016. The influence of fines content and size-ratio on the micro-scale properties of dense bimodal materials. Granul. Matter. 18 (3), 52.

Shire, T., O'Sullivan, C., Hanley, K.J., Fannin, R.J., 2014. Fabric and effective stress distribution in internally unstable soils. J. Geotech. Geoenviron. Eng. 140 (12), 04014072.

Sibille, L., Marot, D., Sail, Y., 2015. A description of internal erosion by suffusion and induced settlements on cohesionless granular matter. Acta Geotech. 10 (6), 735–748.
Skempton, A.W., Brogan, J.M., 1994. Experiments on piping in sandy gravels. Géotechnique 45 (3), 565–567.
Slangen, P., Fannin, R.J., 2017. A flexible wall permeameter for investigating suffusion and suffosion. Geotech. Test. J. 40 (1), 1–14.
Stewart, R.A., Watts, B.D., 2000. The WAC Bennett dam sinkhole incident. In: Proceedings 53rd Canadian Geotechnical Conference, Montreal, Canada.
Thevanayagam, S., Mohan, S., 2000. Intergranular state variables and stress–strain behaviour of silty sands. Géotechnique 50 (1), 1–23.
Thevanayagam, S., Shenthan, T., Mohan, S., Liang, J., 2002. Undrained fragility of clean sands, silty sands, and sandy silts. J. Geotech. Geoenviron. Eng. 128 (10), 849–859.
Xiao, M., Shwiyhat, N., 2012. Experimental investigation of the effects of suffusion on physical and geomechanic characteristics of sandy soils. Geotech. Test. J. 35 (6), 890–900.
Yamamuro, J.A., Lade, P.V., 1997. Static liquefaction of very loose sands. Can. Geotech. J. 34 (6), 905–917.
Yamamuro, J.A., Covert, K.M., 2001. Monotonic and cyclic liquefaction of very loose sands with high silt content. J. Geotech. Geoenviron. Eng. 127 (4), 314–324.
Yasuda, S., Shimizu, Y., Deguchi, K., 2016. Investigation of the mechanism of the 2015 failure of a dike on Kinu River. Soils Found. 56 (4), 581–592.
Zou, Y., Chen, C., Zhang, L., 2020. Simulating progression of internal erosion in gap-graded sandy gravels using coupled CFD-DEM. Int. J. Geomech. 20 (1), 04019135.